A NONGREY CO_2-H_2O GREENHOUSE MODEL OF VENUS

James B. Pollack

June 1968

Smithsonian Institution
Astrophysical Observatory
Cambridge, Massachusetts 02138

A NONGREY CO_2-H_2O GREENHOUSE MODEL OF VENUS

JAMES B. POLLACK
Smithsonian Astrophysical Observatory, Cambridge, Massachusetts 02138

Communicated by Carl Sagan

Received

Nongrey greenhouse calculations are performed with CO_2, H_2O, and N_2 as sources of the infrared opacity. Solar-energy deposition within the various atmospheric layers and at the ground is explicitly calculated. The pressure-induced transitions of N_2 are found to be an unimportant source of opacity for the models considered. The atmospheric region between the bottom of the clouds and the surface exhibits an adiabatic profile, and about 0.5% of water vapor is required to achieve the desired greenhouse effect. Both these results are compatible with the Mariner 5 and Venera 4 results.

This is the fourth in a series of papers concerned with the greenhouse effect on Venus. In the first (Pollack, 1968 - Paper I), equations were developed to treat the relevant radiative transfer processes; in the second (Sagan, 1968 - Paper II), a comparison was made between grey and nongrey temperature gradients and greenhouse effects; and in the third (Sagan and Pollack, 1968 - Paper III), various observations, including the recent spacecraft experiments, were analyzed to obtain information about the structure and composition of the Venus atmosphere. Here we perform nongrey greenhouse calculations for model atmospheres possessing infrared opacity due to carbon dioxide, water vapor, and nitrogen. We wish to determine the

structure of the lower atmosphere of Venus as well as to obtain the water-vapor mixing ratios needed to achieve the desired greenhouse effect.

Evidence that the surface temperature of Venus is substantially higher than the temperature at which it radiates to space was first supplied by the high fluxes seen at radio wavelengths. The spectral distribution of the radio brightness temperature (Barrett and Staelin, 1964), the Mariner 2 radio limb-darkening observations (Barath et al., 1964), interferometric observations (Clark and Kuz'min, 1965), microwave phase-effect measurements (Pollack and Sagan, 1965a), and finally, radar returns (Walker and Sagan, 1966) are consistent with the radio emission arising primarily from a hot surface and lower atmosphere. On the other hand, alternative explanations are inconsistent with one or more of these observations (Pollack and Sagan, 1967a; Walker and Sagan, 1966). In addition, Sagan (1967) pointed out that the apparent difference between optical and radar diameter estimates offers an independent argument in favor of a hot Venus surface. The recent Soviet spacecraft's direct measurement of high atmospheric temperatures on Venus (Pravda, 1967a, 1967b), its high-pressure results, and those of the American Mariner 5 spacecraft (Kliore et al., 1967) confirm these previous conclusions.

We will now summarize the pertinent observational data needed for our calculations and then outline our treatment of the greenhouse problem. After correction has been made for the nonunit emissivity of the surface, an average surface temperature of about 700°K (Pollack and Sagan, 1965a) is implied by the passive radio observations. On the other hand, the Soviet probe found a surface temperature of 543°K on the night side near the equator. It should be pointed out that the lower surface temperature implied by the Soviet observations cannot be attributed to a cooling of the surface at night since at most only a narrow atmospheric boundary layer would be affected by these variations as a result of the large heat capacity of the atmosphere. An extrapolation of the atmospheric temperatures to the surface gives the same value for the surface temperature as the "observed" value (Paper III). The American Mariner 5 space probe was unable to measure the temperature at positions as deep as did the Soviet probe; its highest temperatures were

between 400 and 450°K and were consistent with the Soviet value at a similar pressure (Paper III). We will consider the average surface temperature as lying somewhere between 543°K and 700°K.

Estimates of the CO_2 mixing ratio, based on various theories of line formation, yielded values ranging from less than 1% (Chamberlain, 1965) to almost 100% (Belton and Hunten, 1967). The Soviet spacecraft indicated a mixing ratio of 90 ± 10% by direct measurement of several gas samples, while the stratospheric scale height measured by the Mariner 5 implies, in a less direct fashion, mixing ratios of between about 75 and 90%. The Soviets also obtained an upper limit of 7% on the N_2 mixing ratio. Since N_2 is perhaps the only other gas likely to be present in large amounts in the Venus atmosphere, the most probable value of the CO_2 mixing ratio is between 90 and 100%. A more conservative estimate for the CO_2 mixing ratio places it as 75% or greater. For a fuller discussion of the limits on the CO_2 mixing ratio implied by the spacecraft experiments, see Paper III.

A most important measurement of the Venus 4 spacecraft was a positive detection of water vapor (Nature, 1967). Its mixing ratio has been estimated as lying between 0.1% and 0.7%. The Soviets also claim to have detected between 0.4 and 0.8% oxygen. Finally, from spectroscopic observations, Connes et al. (1967) have detected HCl and HF and found their mixing ratios to be about 6×10^{-7} and 5×10^{-9}.

If we accept the Soviet water-vapor measurement as valid, then there clearly will be an extensive ice-cloud region in the Venus atmosphere (Paper III). It should be noted that the mixing ratios detected were below the saturation value at the level sampled, so the estimated water-vapor mixing ratios apply to the lower atmosphere. The great weakness of the water-vapor lines formed above and in the cloud layer has been used as an argument against the presence of ice clouds (Belton and Hunten, 1967). However, the Mariner 5 data imply that line formation occurs principally at the stratospheric temperature and so very weak lines are expected (Paper III). The low reflectivity of Venus, between 3.0 and 3.3, can be attributed to the ice fundamental at

3.1 μ and provides some evidence in favor of water clouds. Using near-infrared reflectivity observations, Sagan and Pollack (1967) estimated an average particle radius of 7.5 to 10 μ and an optical depth for the hypothesized ice clouds of 18 to 43. More recent size estimates lower the average radius by a factor of 2 or 3 (Pollack and Sagan, 1968). We will assume below that there is a layer of water clouds. Indeed, the water-vapor mixing ratios needed for the greenhouse effect will demand them. We note that the top portion of the clouds will be ice, while the bottom layers may include water droplets.

Infrared limb-darkening observations imply a cloud-top temperature of about 210°K (Pollack and Sagan, 1965b). The Mariner 5 data provide the best estimate of cloud-top pressure. The cloud-top pressure as used in the calculation below refers to that place in the atmosphere where a steep temperature gradient begins abruptly from a zero gradient above. As there is a small but finite region where the gradient increases from zero to a steep value, we cannot obtain the cloud-top pressure exactly from the Mariner 5 data, but we estimate it to be about 230 mb (Paper III). A very generous error limit is ±70 mb. The Mariner 5 data appear to be compatible with previous cloud-top pressure determinations (Paper III). It is not clear whether the cloud layer is a homogeneous region with a constant mixing ratio of cloud particles, in which case a wet adiabatic lapse rate through the clouds would be appropriate, or whether the cloud layer is a series of individual clouds, in which case a dry adiabatic value may be the pertinent lapse rate. We will consider both lapse rates.

In addition to the parameters estimated by the Soviet spacecraft, which are mentioned above, it also found an approximately adiabatic lapse rate between the 310°K and 543°K levels and through extrapolation a pressure of 20 ± 2 atm at the higher temperature point. At the 700°K level, the corresponding pressure is 75 atm (Paper III).

Mariner 5 found the atmosphere to be isothermal above about the 100-mb level, with the temperature gradient changing sharply over to approximately an adiabatic value at all lower levels. There is some indication of a slight subadiabatic lapse rate for the first 20 km of the region of large temperature gradient (Paper III), but this result is somewhat uncertain. We note that this type of behavior would be expected for the first 10 km if a water cloud is present extending to about the 270°K level and possessing a wet adiabatic lapse rate (Paper III).

The decline in the microwave brightness temperature below a wavelength of 3 cm has been attributed to microwave opacity in the atmosphere of Venus. If all the microwave opacity is attributed to CO_2, N_2, and H_2O vapor, a best fit of the microwave spectral data implies a relationship between the mixing ratios of these gases, a_{CO_2}, a_{N_2}, a_{H_2O}, and the surface pressure P_s (Ho et al., 1966):

$$X \equiv P_s^2(15.7a^2_{CO_2} + 3.90a_{CO_2}a_{N_2} + 0.085a_{N_2} + 1330a_{H_2O})$$

$$= 6.33 \times 10^3 \quad . \tag{1}$$

Alternatively, if we attribute the small value of the radar cross section at 3.6 cm (Karp et al., 1964) solely to atmospheric absorption and again assume that CO_2, N_2, and H_2O vapor are the only microwave absorbers, then a value for X of about 6.33×10^4 would be implied. Such a value may be viewed as an upper limit on X for plausible models of the Venus atmosphere. For all successful greenhouse models we will estimate the value of X as well as the fraction of the opacity due to H_2O vapor.

From measurements of the reflectivity of Venus at various wavelengths and phase angles, Sinton (1963) estimates the bolometric albedo is 0.73, which corresponds to an equilibrium temperature of 235° K. Bolometric albedos of between 0.69 and 0.75 and effective temperatures between 232 and 244°K have been inferred by Walker (1966) from measurements at one phase in a

number of different wavelength regions. These values are very similar to estimates of the infrared temperatures of Venus at 3.75 μ of 234°K (Sinton, 1963), between 8 and 13 μ of 225°K (Sinton and Strong, 1960), and at 20 μ of 240°K (Low, 1965). Since the Venus atmosphere above the clouds can be expected to be fairly transparent at these wavelengths, the above temperature also provides an estimate of the temperature at which the clouds radiate to space.

The decline in the albedo of Venus below 4000 Å cannot be attributed to absorption by ice particles; their absorption coefficient is much too low. Rather, we must attribute the absorption to some as yet unidentified component of the atmosphere. We will show below that most of the absorption takes place in the vicinity of the cloud layer.

In the next section, we will estimate the bolometric albedo, as well as the amount of solar energy deposited in the cloud layer, in various layers of the atmosphere, and at the ground. Next, we will calculate the amount of energy radiated by the planet to space and compare this value with that implied by the bolometric albedo in order to ensure that a heat balance occurs between the solar energy absorbed and that radiated to space. The main efforts of this paper will be directed toward calculating a series of greenhouse models for various gas amounts and pressures. In particular, we wish to find the carbon dioxide and water-vapor mixing ratios needed for the greenhouse effect, the lapse rate in the lower atmosphere, and the microwave opacity implied by each model. All these calculations will be based upon the nongrey equations developed in Paper I. Finally, we will summarize the findings of our calculations and discuss the results of other investigators who have dealt with the greenhouse problem for Venus.

I. SOLAR ENERGY DEPOSITION

We wish to calculate the fraction of the incident solar energy that is absorbed by Venus, as well as the distribution of the deposited sunlight throughout the atmosphere. Account must be taken of absorption and

scattering by atmospheric gases, cloud particles, and the ground. In Paper I, approximate formulas to treat such a situation have been presented. We now specify the various parameters needed to carry out the calculations for Venus, as well as to state the assumptions involved.

We first consider those wavelengths at which gaseous absorption may be neglected. For this case, Eqs. (52), (53), and (54) of Paper I determine the fraction of the monochromatic solar energy that is absorbed at the ground, $f_a(g)$, absorbed by the clouds, $f_a(c)$, and reflected to space, f_r. These equations were derived under the assumption that no Rayleigh scattering occurs above the cloud layer, a good assumption for the cloud pressures and wavelengths of interest, and that the ground albedo is zero. According to Eqs. (52), (53), and (54), $f_a(g)$, $f_a(c)$, and f_r are functions of the transmissivity $\mathcal{T}$, reflectivity A_c, and absorptivity B of the clouds as well as the transmissivity t, of the Rayleigh-scattering layer. Equations for $\mathcal{T}$, A_c, and B, are given in Sagan and Pollack (1967); they depend upon the optical depth of the cloud t_λ, a parameter 2β, which indicates the forward-scattering asymmetry of the phase function, and the single scattering albedo $\tilde{\omega}_0(\lambda)$, which is a function of the particle size and absorption coefficient of the cloud material. An approximate equation for $\tilde{\omega}_0$ is given in the same paper when the size is large compared to the wavelength. In evaluating $\mathcal{T}$, A_c, and B, we assumed the cloud particles were ice crystals with a mean particle radius of 7.5 μ and that the optical depth of the clouds in the visual lie between 18 and 43, for reasons given in the introduction. The optical depth at any other wavelength can be found by scaling of the extinction cross section Q_{ext}, while 2β equals $1 - \langle \cos\theta \rangle$, where $\langle \cos\theta \rangle$ is the average cosine of the scattering angle. The parameters Q_{ext}, $\tilde{\omega}_0$, and $\langle \cos\theta \rangle$ were obtained from Mie scattering calculations by Irvine and Pollack (1968) for small ice spheres. These same authors also provide values for the absorption coefficients of ice. When the particle is large compared with a wavelength Q_{ext}, $\langle \cos\theta \rangle$ and, to a lesser extent, $\tilde{\omega}_0$, show an oscillatory behavior when evaluated for a single-particle size, as was the case for the Irvine and Pollack estimates. The oscillatory behavior is greatly damped when a particle-size distribution is

allowed for and so we used average values of Q_{ext} and $\langle \cos \theta \rangle$ and the formula in Sagan and Pollack for $\tilde{\omega}_0$ when the size was large compared to a wavelength. Equations (55) and (56) of Paper I specify the transmissivity of the Rayleigh-scattering layer t, in terms of the surface pressure for a pure N_2 atmosphere. Calculations will be performed for surface pressures of 15 atm, 75 atm, and 300 atm. The corresponding pressures for a pure CO_2 atmosphere that will yield the same results are 10, 50, and 200 atm, respectively.

We next consider the calculation of the amount of solar energy absorbed by the atmospheric gases. Both CO_2 and H_2O vapor can be expected to absorb a significant fraction of the incident solar beam. Equations (57) and (58) of Paper I provide estimates of the equivalent width $\Delta\tilde{\nu}$ for absorption by a band or several nearby bands. The quantity $\Delta\tilde{\nu}$ gives the equivalent width for all the absorption that takes place between the top of the atmosphere and the end of a given path length, characterized by a gas of amount W and pressure P. The value W is proportional to the integral of the absorbing gas density over the path length of interest. We will use a W weighted average value for P, which equals half the end-point pressure when the path is a direct one, since $W \propto P$ by hydrostatic equilibrium. Because of the nonlinear dependence of $\Delta\tilde{\nu}$ on W, all calculations must have as the starting point the top of the atmosphere. Similarly, after the solar beam is reflected by or transmitted through the clouds, it must be diminished by a factor of A_c or $\mathcal{T}$. By taking the difference between the value of $\Delta\tilde{\nu}$ for two end points, we can obtain the value of $\Delta\tilde{\nu}$ appropriate for absorption between those two levels. For direct paths, we assume that on the average W equals twice its value for a vertical path. Finally, when there is much scattering, such as in the cloud layer, we increase the path by $2\beta\tau$. See Paper I for a detailed discussion of this point. (Fortunately, little correction is needed for Rayleigh scattering because of the long wavelengths at which gaseous absorption takes place, and no correction was made in the calculations performed.)

As an example of our approach, suppose we wish to calculate the amount of solar energy absorbed in a particular band between levels A and B after reflection by the clouds. We calculate $\Delta\tilde{\nu}_A$ and $\Delta\tilde{\nu}_B$ for paths first down to the tops of the clouds and then up to the level of interest. The amount of solar energy absorbed by the band between A and B after reflection from the clouds equals $F_{\tilde{\nu}} A_c(\Delta\tilde{\nu}_A - \Delta\tilde{\nu}_B)/4$, where $F_{\tilde{\nu}}$ is the solar flux at normal incidence expressed in units of cm^{-1}, A_c is the cloud albedo, and the factor of 4 represents the result of averaging the solar flux over the day and night side. To obtain the total solar energy absorbed by the band between levels A and B we must add on $F_{\tilde{\nu}}(\Delta\tilde{\nu}'_B - \Delta\tilde{\nu}'_B)/4$, where $\Delta\tilde{\nu}'$ is evaluated for paths directly down to levels A and B and represents the solar energy absorbed before reaching the cloud layers.

To carry out the calculation of gaseous absorption, we must first find the values of the empirical constants appearing in Eqs. (57) and (58), as well as the boundary point $\Delta\tilde{\nu}_\ell$, which indicates the appropriate formula to be used. Howard et al. (1956) and Burch et al. (1965, 1966) are our basic sources of information for these parameters. Unfortunately, for the Howard et al. parameter specification, $\Delta\tilde{\nu}_{s,w}$ does not exactly equal $\Delta\tilde{\nu}_{s,s}$ at the boundary point $\Delta\tilde{\nu}_\ell$. To remedy this situation, we demanded that k be such that k/d equal K/D, a condition nearly met by the original data, and redetermined c so that $\Delta\tilde{\nu}_{s,s}$ would exactly equal $\Delta\tilde{\nu}_{s,w}$ at $\Delta\tilde{\nu}_\ell$.

For a number of bands – 1.44 and 1.59 μ CO_2, 0.926, 1.14, and 3.26 μ H_2O – values of the empirical parameters are given for the strong-line, weak-band region (sw), but none of the strong-line, strong-band region (ss). We attempt to estimate C, D, and K in the following manner. As above, one relationship is supplied by setting K/D equal to k/d. A second equation involving C, D, and K follows similarly by $(\Delta\tilde{\nu})_{s,w}$ being set equal to $(\Delta\tilde{\nu})_{s,s}$ at $(\Delta\tilde{\nu})_\ell$. (Values of $\Delta\tilde{\nu}_\ell$ are given by Howard et al. for these bands.) Ohring et al. (1964) have suggested that a third relationship could be obtained by trying to find a linear relationship between C and D from the bands for which these parameters have been determined. While a weak linear relationship is suggested by the CO_2 data, this is certainly not the case for the H_2O

data, as detailed calculations show and as is evident from Table 1 (C and D are given by Howard et al. for the 6.25, 2.58, 1.87, and 1.38 μ H_2O bands). A third relationship is suggested from Eq. (58) if we note that for very large values of $WP^{K/D}$, $(\Delta\tilde{\nu})_{s,s} \propto D$. This suggests D should be related to the limits of the various bands. We tried a proportionality relationship between D and the band limits: $D = \underline{a}(\tilde{\nu}_1 - \tilde{\nu}_2)$, where $\tilde{\nu}_1$ and $\tilde{\nu}_2$ are the band limits and $\underline{a}$ is a constant. The parameter $\underline{a}$ was determined separately from each known value of D. For the H_2O bands, $\underline{a}$ was found to be 0.24, 0.23, 0.21, and 0.31 for an average value of 0.25, while for the CO_2 band, $\underline{a}$ was 0.22, 0.10, 0.24, and 0.31 for an average value of 0.22. While there is a moderate dispersion in the individual values of $\underline{a}$, it is not too large. It is interesting to note that the average values of $\underline{a}$ for the CO_2 and H_2O bands are quite similar.

Finally, no data are given in Howard et al. for the very weak 1.06 and 1.22 μ CO_2 bands and the 0.813 and 0.719 μ H_2O bands. However, Burch et al. (1965, 1966) have recently finished a study of these bands and kindly furnished us with preprints of their data. Their data provide values for c for these bands, and the band limits are known. Since d and k are quite similar for various bands of a given gas, we used the values of the nearest known band. Finally C, D, and K were determined by the method outlined above.

Table 1 summarizes the values of the empirical parameters as determined above. Because of a lack of data at high temperatures, all these parameters have been evaluated for 300°K, and no attempt has been made to apply temperature corrections or to consider hot bands that could be important at higher temperatures. As we will see later, inclusion of temperature corrections will not affect our basic results. We can calculate the total amount of sunlight absorbed by the atmospheric gases, the energy absorbed between any two levels in the atmosphere, and the amount absorbed below a particular level.

Our basic procedure is to calculate the values of $f_a(g)$, $f_a(c)$, f_r, and A_c for all wavelengths above 4000 Å and similarly to obtain the values for $\Delta\tilde{\nu}$. Overlapping by neighboring gaseous absorption bands is corrected for by assuming a square-wave distribution for the absorption in wave-number space. Finally, all wave-number integrations are weighted by the wave-number distribution of solar energy, with the integration for the amount of sunlight absorbed by the ground and cloud aerosols carried out only over the regions between absorption bands. The absorption below 4000 Å is due to an unknown absorber, and the absorption was evaluated directly from the observed albedos (Sinton, 1963; Evans et al. 1965). We denote this component of absorption by x.

Figures 1, 2, and 3, exhibit the monochromatic albedo of Venus, in the absence of gaseous absorption $\mathcal{R}_\lambda$, the absorptivity of the clouds B_λ, and the transmissivity of the clouds $\mathcal{T}_\lambda$. Figure 1 shows that beyond 1 μ the curves for a fixed optical depth of the clouds show little surface-pressure dependence and hence almost all the observed albedo is derived from the clouds. Moroz (1963) finds that the ratio of the continuum albedo at 1.2 μ to that at 5500 Å is about 0.9, and so the cloud itself has an intrinsically high albedo. Such an albedo ratio is compatible with the computed curves shown in Fig. 1 for surface pressure permitted by the recent spacecraft experiments. We also see from this figure that below 4000 Å the predicted albedo approaches unity, in severe disagreement with the observations. This indicates the presence of some additional absorber, which furthermore is neither CO_2 nor H_2O. Since the ratio of the reflectivity at 3500 Å to that at 5500 Å is 0.61, which is significantly lower than the ratio that would pertain if the absorber were completely below the clouds and so affected only the Rayleigh-scattering component, the absorber must exist partially above the bottom of the clouds. We will tentatively assume that all the absorption below 4000 Å takes place above the cloud bottoms.

Figure 2 shows that the cloud aerosols do not absorb an appreciable fraction of the sunlight except for wavelengths in excess of 1.5 μ. However, there is still a significant amount of sunlight beyond 1.5 μ, and so some solar

energy will be deposited in the water particles. Even though the cloud begins to absorb beyond 1.5 μ, according to Fig. 3 it is not until 2.7 μ that they become very opaque and transmit little radiation. In Table II we provide estimates of the wavelength regions free from gaseous absorption along a path stretching from the top to the bottom of the atmosphere. In these windows sunlight will reach the surface. Gas mixture B denotes a mixing ratio of 10^{-3} for CO_2 and 8.6×10^{-4} for H_2O vapor in the lower atmosphere, while gas mixture A refers to a mixing ratio of 10^{-1} and 9.6×10^{-3}, respectively. It is interesting to notice how insensitively the size of the window region depends upon the mixing ratio chosen. This is because the bands are either very weak or on the logarithmic parts of their curve of growth. The second column of Table II is the one closest to the conditions found by Venera 4. We see that almost all of the solar energy beyond 1 μ and some of that between 0.7 μ and 1 μ will be absorbed before reaching the ground. Nevertheless, since the biggest window regions are located near the peak of the solar-energy distribution, the ground will be able to absorb an appreciable amount of sunlight. In other words, the Venus atmosphere is not completely black to sunlight, and the greenhouse is therefore not completely "dirty."

Calculations of solar-energy deposition were carried out for a variety of cloud optical depths τ, surface pressures P_s, and gas amounts. In all cases, the cloud-top pressure was taken as 200 mb. Table III summarizes the distribution of the deposited solar energy among the various sinks: The atmosphere a, ground g, cloud aerosols c, and unknown absorber x. The parameter n denotes the fraction of energy deposited in a given sink and is normalized by the total amount of sunlight absorbed, in contrast to the total amount of sunlight incident upon the planet. Also given are the total fraction of energy absorbed in the cloud layer $n'(c)$, which is the sum of the aerosol fraction and the gaseous fraction within the cloud layer, the fraction of sunlight absorbed above the cloud layer $n'(a)$, and the fraction absorbed by the atmosphere below the cloud layer $n''(a)$.

For a fixed pressure, the difference in the distribution of solar-energy deposition between the various cases arises mostly from a variation in the optical depth of the clouds rather than the gaseous mixing ratios: When the optical depth is increased, less light is transmitted through the clouds to be absorbed by the atmosphere beneath or by the ground. Similarly, the major difference in the amount of sunlight absorbed at the ground is attributable both to variations in the optical depth of the clouds and the optical depth for Rayleigh scattering, which is important at the major window regions.

A parameter of great importance for later calculation is the fraction $f(z_c)$ of the deposited energy that is situated below the cloud layers. As the unknown absorber in the UV absorbs entirely above the bottom of the clouds, $f(z_c)$ will simply equal $n(g) + n''(a)$. From Table III, we see that $f(z_c)$ varies only very slowly with large changes in surface pressure and in the mixing ratios of CO_2 and H_2O and is somewhat more sensitive to the choice of the optical depth of the clouds.

Table IV gives a detailed breakdown of the location of the solar-energy deposition. It gives the fraction Δh of the absorbed sunlight that is deposited in a given level of the atmosphere per unit pressure. For example, with $P_s = 15$ atm, $\tau = 18$, and case A, 1.5% of the total deposited sunlight resides in level 8 per unit pressure, and so 4.5% altogether lies within level 8 as level 8 spans the region from 2-atm pressure to 5 atm. An important feature of Table IV is that the solar flux declines only very slowly with increasing depth below the cloud layer. Let us consider case A, $P_s = 15$ atm, $\tau = 18$ and suppose all the energy deposited in x lies above the bottom of the clouds. Then 62.7% of the deposited energy will be placed below the cloud bottom, 55% will be situated below the 2-atm level, 50.4% below the 5-atm level, 46.9% below the 10-atm level, and finally 43.7% will be positioned in the ground. One consequence of this slow decline, as we will see in Section III, is that it is the total solar flux deposited below the cloud that determines the greenhouse effect, and not the amount deposited at the ground. We see that a substantial amount of sunlight is deposited below the cloud layer.

Table V exhibits the bolometric albedo, i. e., the fraction of solar energy reflected to space, and the effective temperature of the planet for each model. The effective temperature is the average temperature at which Venus must radiate to space to lose an amount of energy equal to the amount of sunlight absorbed. The formulas used are given in Blanco and McCuskey (1961). We see that the values of the bolometric albedo are quite similar to the more directly observed value of approximately 0. 73.

II. ESTIMATES OF THE ENERGY BALANCE

In the last section, we estimated how much solar energy was absorbed by Venus. We now wish to calculate how much infrared radiation Venus radiates to space and see how comparable these two figures are. In principle, they should exactly agree, but because of an uncertainty as to the choice of certain parameters, we can demand only approximate agreement. That this will be the case is readily seen: Fig. 3 shows that for all wavelengths in which there is an appreciable amount of infrared energy — 3 μ to 100 μ— the clouds of Venus are extremely opaque, and thus the effective temperature of emission to space will be close to that of the effective emitting temperature of the clouds, 235° K. The effective temperature will actually be somewhat lower because of the presence of gaseous opacity in certain infrared wavelength regions.

To perform the infrared flux calculation, we must first ascertain the parameters c_{ij}, r_{ij}, s_{ij}, that appear in Eq. (13) of Paper I for the opacity of gas j in the wavelength interval i. The broad-band opacity τ_{ij} is a transmission average opacity, as defined in Eq. (3) Paper I. We will be concerned with three sources of gaseous opacity: H_2O, CO_2, and N_2. The N_2 molecule is homonuclear and so its infrared transitions are forbidden. However, at sufficiently high pressure, a pressure-induced dipole moment will be present. While in principle the opacity parameters can be derived directly from low-resolution laboratory spectra, in practice some wavelength regions necessitated path lengths as yet unachievable in the laboratory. In

addition, certain wavelength intervals susceptible to laboratory measurement have not been investigated for a broad enough range of pressure and gas amount, and future work in this area would be highly valuable.

Our basic source of data for CO_2 was broad-band transmission values theoretically calculated by Stull et al. (1963) at pressures of 1 atm and lower, and by Plass and Wyatt (1962) for pressures up to 31 atm. The transmission averages were calculated for a wide range of gas amounts. Below 8.9 μ we employed the transmission calculations of Wyatt et al. (1962) to obtain the relevant parameters for H_2O vapor. Between 8.9 and 12.9 μ, we utilized the empirical formula given by Davis and Viezie (1964), while for the longer wavelength domains, laboratory data by Stauffer and Walsh (1966) and by Palmer (1960) were fitted to Eq. (6) of Paper I. Finally, Solomon (1966) has kindly provided us with a graph of the monochromatic opacity for a hypothetical atmosphere consisting of 90 atm of N_2 and 10 atm of CO_2. We note that pressure-induced transitions show no rotational fine structure and that the monochromatic opacity varies quite smoothly with wavelength. Since the monochromatic opacity of pressure-induced transitions scales as pressure squared, or more correctly, pressure times gas amount, Solomon's opacity can be generalized to a variety of hypothetical atmospheres and r will equal s.

All the above data refer to a temperature of 300° K. Unfortunately, there are not enough data at higher temperatures to allow for possible temperature dependence. The one exception and an important one is that we can readily allow for the temperature variation when the dominant sources of opacity in a given interval at 300° K are hot bands. This is the situation for the 8.9 to 12.9 μ region for CO_2, which is dominated even at 300° K by the 9.4 μ and 10.4 μ hot bands. We simply set $G_i^{1/ri}$ equal to the Boltzmann factor with the energy appropriate for these bands and normalized so that $G_i^{1/ri} = 1$ at 300° K.

Tables VI, VII, and VIII summarize the value of r, s, and c found in the above manner. The values of c given in these tables are appropriate when the pressure has units of atmospheres and the gas amount has units of cm atm for CO_2, pr. cm for H_2O, and 1.11 atm for N_2. Two estimates of r, s, and c have been made from pairs of transmissivity values; one being near 1/2 and the second pair having much lower transmissivity values. The former quantities are labeled without primes, while the latter are denoted with primes. Primed and unprimed values of r represent transmission values spanning several orders of magnitude differences in gas amounts, while pairs of s values generally cover only an order of magnitude difference in the values of pressure, with a maximum pressure of 1 atm. Three important exceptions to the pressure values investigated are regions 6 and 7 for CO_2, which span pressures between 1 and 31 atm, and region 8 for CO_2, which spans pressures between 0.2 and 31 atm. The values of c and c′ were obtained from the same data used to calculate r and r′, respectively. To some extent, the difference between c and c′ is due to the change in the value of r, rather than to a change in the opacity as calculated by the original formula. To estimate how much the opacity itself has changed, we have calculated the quantity W_c, which is the gas amount required for the transmissivity to equal 1/2 along a path at a constant pressure of 1 atm. We see that generally r, s, and W_c change very slowly with pressure and gas amount so that opacity Eq. (13) should be fairly accurate when used as an interpolation formula, and this equation will still have some validity as an extrapolation formula. In all the calculations below we will use the unprimed values since they interpolate the transmissivity at those optical depths contributing most to the flux. We see that for many intervals $r \approx s$ as was expected from the discussion in Paper I.

Equation (4) of Paper I is now used to calculate the flux radiated to space in each wavelength interval. We note that the wavelength intervals in Tables VI through VIII span the region from 2 to 100 μ. Such a wide range is needed to ensure adequate coverage of the blackbody function. Equation (13) is used to calculate the opacity in a given wavelength interval for a specified gaseous absorber, and then we sum over the three sources of opacity to obtain the total opacity. We approximate the radiative transfer process for the

cloud layer by localizing the cloud opacity at the 235° K temperature level and assuming it to be infinite. The atmosphere is assumed to be adiabatic from the 235° K level to the 210° K level, above which the atmosphere is assumed to be isothermal.

Table IX summarizes the results of the flux calculations for individual wavelength regions by assigning an effective temperature at which a blackbody would produce the same amount of flux as is actually emitted. The calculation was performed for two CO_2 mixing ratios, 0.1% and 10%. Water vapor was assumed to be present at saturation values throughout the adiabatic portion of the atmosphere. Again, the pressure at the bottom of the isothermal region was taken as 200 mb. We see that the opacity of the atmosphere above the clouds has become small in many wavelength regions, owing to the precipitation of water vapor as well as the temperature sensitivity of the 9.4 and 10.4 μ hot bands. In particular, we see that in the wavelength intervals 3.42 to 3.88 μ, 8.89 to 12.90, and 17.39 to 29.41 μ, where the temperature has been measured, the effective temperature is close to the cloud temperature. Thus, in the first approximation we can identify the measured temperature with the cloud temperature, as was done in the introduction of this paper.

Summing over all wavelength intervals, we can derive an integrated flux and from that an effective temperature for the thermal radiation to space. We find a value of 225.4° K for the 10% CO_2 case, and 227.4° K for the 0.1% case. We note the great insensitivity of these numbers to the CO_2 mixing ratio assumed. An uncertainty of ±10° K is attached to these calculations, which is derived mostly from an uncertainty in the effective cloud temperature. This temperature can be compared with a value of 235° K, with a similar uncertainty, derived from the bolometric albedo and summarized in Table V. The two results are equal within their uncertainties. These calculations may be viewed as showing that the cloud-top temperature, and more generally the temperature throughout the cloud, are controlled by the heat-balance requirement.

III. TEMPERATURE STRUCTURE OF THE VENUS ATMOSPHERE AND REQUIREMENT FOR THE GREENHOUSE EFFECT

We wish to estimate the amount of CO_2, H_2O, and N_2 needed to produce a very efficient greenhouse effect and to find the temperature lapse rate in the region between the bottom of the clouds and the surface. In Paper I we discussed why the clouds can be expected to mark the end of the convection zone in the lower atmosphere. We showed that the temperature gradient near the cloud bottom is not necessarily indicative of the gradient in deeper and so in principle there could be only a local convection zone near the cloud bottoms. The demand that the clouds exist at the end of the convection zone enables us to specify the temperature gradient ψ, as will be done below, and so from Eqs. (33) and (36) of Paper I for the net infrared flux at the cloud bottom we can obtain a constraint on the opacity. With this constraint we can then find the radiative temperature gradient in deeper portions of the atmosphere from Eq. (26) of Paper I and, finally, calculate the microwave opacity of the atmosphere.

We now consider the flux equation at the bottom of the clouds in more detail. The quantity $F(z)$ simply equals $f(z)\,\sigma T_e^4$, where σ is the Stefan-Boltzmann constant, T_e is the effective temperature, which we take as 235° K, and $f(z)$ is the fraction of the deposited sunlight, which is absorbed below level z, here the cloud bottoms. The calculations of Section I indicated that $f(z)$ was very insensitive to the choice of gas amount or surface pressure and we will use an average value of 0.525, implied by Table III for a surface pressure of 15 atm. If we assume that the effective emitting temperature of the clouds in a downward direction T_c equals the thermometric cloud-bottom temperature, then according to Eq. (35) of Paper I there will be a temperature discontinuity at the cloud bottoms for the radiative equilibrium solution. If ΔT denotes this discontinuity and if we assume that the radiative lapse rate is half the adiabatic value from the air cloud-bottom temperature $T(z)$ to $T(z) + \Delta T$, then when convective instability is allowed for, the temperature

will go from T_c to $[T(z) + \Delta T]$ over the same region of the atmosphere and the gradient will be adiabatic. We note that our calculations are very insensitive to the exact specification of the boundary-layer radiative lapse rate. We further assume that the radiative lapse rate is the adiabatic value below the boundary region so that the clouds mark the end of the convection zone. We note that because the clouds act as a blackbody at the upper boundary, the stratospheric-structure problem is decoupled from the tropospheric problem.

A number of simplifying assumptions entered into the derivation of Eq. (36) of Paper I from the rigorous integral form of the flux equation. Sample calculations indicate that the use of Eq. (36) gives rise to errors of less then 15%, which was considered adequate for our purposes.

We now consider the number of free parameters entering into Eq. (36) of Paper I. The quantities f(z) and ψ have been specified above; $\bar{Z}_i$ is defined by Eq. (33) of Paper I. Since θ_j is proportional to the mixing ratio of gas j, and B_i is a function of temperature, which in turn is related to pressure through ψ, there are essentially five free parameters: The mixing ratio of the three gases under consideration, the total pressure at some reference level, and the cloud-bottom temperature. Since H_2O, CO_2, and N_2 can be assumed to be the principle constituents of the Venus atmosphere, the sum of their mixing ratios must be one. In addition, the partial pressure of water vapor at the cloud bottoms will equal the saturation value, which is a function only of the cloud-bottom temperature T_c. Thus, only three independent parameters enter into Eq. (36). For a given model we select two of these parameters and use Eq. (36) to find the third.

We choose as the two specifiable parameters the cloud-top pressure $\tilde{P}$, for which we have various measurements, and the cloud-bottom temperature T_c. The CO_2 mixing ratio a_{CO_2}, is then inferred from Eq. (36). The values of c, r, and s contained in Tables VI, VII, and VIII are used in the calculations.

We choose to determine the CO_2 mixing ratio a_{CO_2} from the cloud-bottom flux equation because the atmosphere in its vicinity is at conditions close to STP, where the values of c, r, and s are most well known and where our use of Tables VI, VII, and VIII will be mostly an interpolation procedure. For this reason, we feel the determination of a_{CO_2} from the flux at the bottom of the atmosphere is far less desirable. In order to extrapolate the cloud-top pressure to the cloud bottom and thence to lower altitudes, we must first know the lapse rate within the clouds. From the monochromatic transmissivity of the clouds, summarized in Fig. 2, we can readily calculate the Rosseland mean opacity of the clouds for a typical cloud temperature of 240° K. We find this to be 6 for a visual extinction optical depth of 18 and 13 for a visual value of 43. If the cloud layer is well mixed and the cloud-top temperature is 210° K, these optical depths would imply cloud-bottom temperatures of 375° K and 450° K, respectively, under the assumption of radiative equilibrium. Since lower cloud-bottom temperatures will be considered in our models, such clouds would be in convective equilibrium with a wet adiabatic temperature gradient, i.e., one that allows for the release of latent heat. Relevant formulas for the wet adiabatic lapse rate are contained in Hess (1959). Similarly, if the clouds occur in discrete layers with radiative exchange between them, we can again expect an adiabatic lapse rate, although it may be a dry one. We will employ both lapse rates to extrapolate the cloud-top pressures. The cloud-top temperature is taken to be 210° K.

We now use the values of the specified parameters as well as the CO_2 mixing ratio inferred from the flux equation at the cloud bottoms to calculate the radiative value of ψ at a pressure level 6 times that of the cloud bottoms. An adiabatic lapse rate is used to find the temperature at this point from the atmospheric parameters at the clouds. Equation (26) of Paper I is used to perform the calculation of ψ. If the radiative value of ψ is greater than $\gamma/(\gamma - 1)$, where γ is the ratio of the specific heats, the atmosphere is unstable at that position and so assumes the adiabatic value. We then use the actual value to proceed to a level where the pressure is 1.5 times larger than at the present level and the process repeated. We continue in steps of 1.5 until an assumed surface temperature of 700° K is reached. The value of f(z) at each pressure level is found from the calculations in Table IV.

Finally, we estimate the microwave opacity of the atmosphere by calculating the parameters M and R; M is defined as the ratio of the parameter X, defined by Eq. (1) of the introduction, to 6.33×10^3. If CO_2, H_2O, and N_2 are the chief sources of the microwave gravity of Venus, a value for M of 1 gives a good fit to the microwave brightness temperature spectrum, while a value of 10 would account for the low 3.0-cm radar cross section. In any case, M should not be above 10. The parameter R is the ratio of the fourth term of Eq. (1) to the sum of the first three and is thus the ratio of the microwave opacity due to water vapor to that attributable to CO_2 and N_2.

A computer program was constructed by David Ziskind to carry out the above calculations and allow us to explore many possible models. Our approximations made the equations sufficiently simple so that 200 model calculations were carried out in just an hour of computer time.

We now summarize the results of the above calculations. One general property of all models is that the atmosphere is in convective equilibrium from the cloud bottoms to the ground. This result was anticipated in Paper II. Usually the wavelength region contributing the most to the total flux was region 6, characterized by a mean wavelength of 8 μ and thus according to Eq. (21) of Paper I by a value of n of about 4.5 at 400°K. Water vapor was usually the most important contributor to the opacity in this region and so $s/r = 0.8$. The parameters ϵ and ξ are approximately zero. Thus, the radiative value of ψ at the 400°K level is about 0.4 compared to an adiabatic value of about 0.2. As the sample calculation would indicate and as the actual ones showed, the radiative value of ψ was considerably larger than the adiabatic value. Accordingly, the exact value of f(z) is irrelevant for the final structure of the atmosphere as long as it varies slowly with pressure below the clouds, as it did for all the cases considered in Table IV. Similarly, we may have neglected important sources of opacity at high pressures and temperatures, such as hot bands, but these will only lead to larger radiative values of ψ and the resultant atmospheric structure will remain adiabatic. We also see that the greenhouse effect is determined by the value of f(z) at

the cloud bottoms and not by its value at the surface: We can change f(z) at the surface substantially without changing the atmospheric structure. The predicted adiabatic behavior of the lower portion of the Venus atmosphere is in good agreement with the Venera 4 and Mariner 5 results.

The values of W_c, the gas amount needed to achieve a transmissivity of 1/2 at 1 atm pressure, allow us to estimate the wavelength where the opacity will be the least and the contribution to the total flux the greatest. Tables VI, VII, and VIII list the estimates of W_c. For comparison, an atmosphere of 10% CO_2, 1% H_2O, and 89% N_2 would have W_c amounts of 8.7×10^4 cm atm, 7.1 pr. cm, and 0.89 atm, respectively, of these gases above the 1-atm pressure level. Thus, for example, region 4 for CO_2, the region of the 15 μ fundamental, is characterized by a W_c value of 6.5 and certainly will be very opaque unless the CO_2 mixing ratio is exceedingly small. On the other hand, regions 6, 7, 11, and 13 are very transparent for CO_2, and in fact regions 1, 2, and 3, where there is essentially no CO_2 opacity, are completely transparent. Water vapor quite conveniently is fairly opaque at a number of these transparent regions for CO_2, as indicated by Sagan (1960). In regions 1, 2, and 3 it is very opaque. Here the pure rotation band of H_2O vapor is situated. Similarly, regions 7 and 11 are fairly opaque for H_2O vapor. Thus, we can see that regions 6 and 13 will be the most transparent ones for a mixture of H_2O and CO_2. Because region 6 is closer to the peak of the blackbody function than is region 13, except perhaps at the bottom of the atmosphere, region 6 can generally be expected to be the one most contributing to the total flux and the region most influencing the greenhouse calculations. This fact was first pointed out by Sagan (1960). Comparing Tables VI and VII with Table VIII, which gives the regions in which N_2 pressure-induced opacity is the strongest, we see that in regions 1, 2, and 3 the pressure-induced rotational opacity of N_2 will generally be small compared to the permitted rotational opacity of H_2O vapor, and similarly, in region 9, the pressure-induced fundamental of N_2 will generally be insignificant compared to the 4.3 μ CO_2 fundamental.

The above deduction, that the N_2 pressure-induced transitions are generally unimportant, is borne out by the calculations. Even with a cloud-bottom temperature as low as 240° K and water-vapor mixing ratios as low as 10^{-5}, the water-vapor opacity still dominates in regions 1, 2, and 3, and a similar statement holds for CO_2 and N_2 in region 9. A somewhat surprising fact is that the N_2 pressure-induced opacity does not become more important at the higher pressure near the surface. In region 1, for example, the N_2 opacity with respect to the top of the atmosphere varies as P^2, while the H_2O opacity, again with respect to the top of the atmosphere, varies approximately as P^1, and so the N_2 opacity will certainly increase faster than the H_2O opacity. However, the opacity between two nearby levels in the atmosphere will not reflect this type of opacity pressure dependence because of the non-linear dependence of the H_2O opacity on gas amount, as is explained more fully in Paper I. According to Eq. (26) of Paper I, the ability of a given gas component to reduce the IR flux varies as $P^{(s/r+1)}$, and so the ability of H_2O and N_2 to reduce the IR flux will change very little with depth in the atmosphere. Table X illustrates this point by comparing the value of Y for CO_2, N_2, and H_2O near the cloud bottoms and near the surface; Y denotes the value of the quantity within the inner parenthesis of Eq. (26) of Paper I and provides a measure of the importance of a given gaseous constituent in controlling the IR flux in a given wavelength interval.

Table VII has an interesting implication about the possibility of H_2O vapor completely dominating the opacity at each wavelength interval. We saw earlier that with 1% H_2O above the 1-atm pressure level there are 7.1 pr. cm of H_2O. We see from the W_c values in Table VII that if the H_2O mixing ratio and the total pressure are sufficiently high, water vapor could by itself completely blanket the entire IR wavelength region. Several models below will explicitly illustrate this possibility. While the mixing ratio and pressure requirements may be too extreme for the present Venus atmosphere, this possibility might have been of some importance in Venus' past history.

Table XI summarizes the results of the greenhouse calculations for a wide variety of cloud-top pressures and cloud-bottom temperatures. The symbols 1 and 0 next to the cloud-bottom temperature denote the use of dry and wet adiabatics throughout the cloud. For temperatures less than 270° K, the results were essentially identical. Not all models were capable of fulfilling flux Eq. (36) of Paper I. One obvious reason for such a failure is that the inferred water-vapor mixing ratio below the clouds exceeds unity. Such a situation arises when the cloud-bottom temperature is high and the cloud-top pressure is low. We denote this kind of model by listing >1 in the a_{H_2O} column of Table X. A second reason for failure is that the opacity may be too low or too high for any acceptable CO_2 mixing ratio. If the cloud-bottom pressure and water-vapor mixing ratio are too small, even a maximum mixing ratio of CO_2, $1 - a_{H_2O}$, will lead to too high an infrared net flux at the cloud bottoms. Such a model is identified by >1 in the a_{H_2O} column. On the other hand, if the cloud-bottom temperature and cloud-top pressure are too high, water vapor by itself may be too opaque. We indicate this model with >0 in the a_{H_2O} column. Because of a combination of factors discussed above, no cloud model with a cloud-bottom temperature of 360° K or greater was successful. When the cloud-top pressure was low, the water-vapor mixing ratio exceeded 1, and when it was raised sufficiently to overcome this difficulty, water vapor became too opaque. Despite all the models that did not work, it is remarkable how wide a range of models was successful; clearly some observational constraints must be placed so as to narrow down the list of possibilities.

As a result of the recent space experiments, we can obtain a fairly specific greenhouse model to compare with the observations. We begin by imposing modest limits on the input parameters and progress to more severe limits. The cloud-top pressure surely lies between 50 and 500 mb, and the CO_2 abundance should exceed 50%. Figures 4 through 9 illustrate the behavior of the other parameters under these constraints. The dashed curves and solid curves correspond to the assumption of a wet and a dry adiabatic lapse rate in the clouds, respectively. The values of P_s, the surface pressure, M, and R are all computed for an assumed surface temperature of 700°K. If the surface temperature is actually 543°K, P_s should be lowered by a factor 4.5,

M by a factor of 20, and R will be unchanged. The space experiments certainly permit more stringent limitation on the input parameters. Table XII summarizes the range of output parameters permitted when the CO_2 mixing ratio is above 75% and the cloud-top pressure lies between 150 and 300 mb. Finally, let us pick the most likely set of input parameters: a cloud-top pressure of 230 mb, a CO_2 mixing ratio of about 97%, and a wet lapse rate in the clouds. The resulting output parameters are again summarized in Table XI.

Let us now consider Table XII in greater detail. A pressure of 100 atm at the 700° K level is implied when the best choice of input parameters is used. This implies a pressure of 22 atm at the 543° level, in excellent agreement with the Venera 4 results of 20 ± 2 atm. A similar agreement could be obtained by choosing a higher cloud-top pressure than 230 mb and lower values of the CO_2 mixing ratio.

For the best-choice case, a water-vapor mixing ratio of about 0.5% is required. This value falls within the range of 0.1 to 0.7% for the water-vapor mixing ratio determined by the Venera 4 experiment. If we lower the CO_2 mixing ratio below 97% and raise the cloud-top pressure above 230 mb so as to achieve the Soviet pressure value at 543° K, we again obtain water-vapor mixing ratios compatible with the Soviet water-vapor results. Similar statements hold for a change from wet to dry lapse rate in the clouds, which also requires an increase in $\tilde{P}$ to match P(T = 543° K). Even with the conditions relaxed to $a_{CO_2} \geq 0.75$ and 150 mb $\leq \tilde{P} \leq$ 300 mb, the water-vapor mixing ratio required for the greenhouse effect is at most a factor of 3 above the Soviet upper limit. Thus it would appear that H_2O and CO_2 are the chief sources of the greenhouse effect on Venus, provided we accept the Russian water measurements as valid.

The cloud-bottom temperatures T implied by the calculation are close to the freezing point of water. Hence, the cloud will consist mostly of ice crystals except near the bottom. The wet lapse rate implied by these temperatures is compatible with the apparently slightly subadiabatic lapse rate inferred from the Mariner 5 results for the region the clouds would occupy

(Sagan and Pollack, 1968). The sharp change in temperature gradient near the 230-mb level was expected by our model. Below 230-mb level there is abundant opacity due to the cloud aerosols, while above the 230-mb level there is only CO_2 absorption in a few wavelength regions and a large amount of solar heating.

The values of R in Table XII show that both CO_2 and H_2O vapor will make similar contributions to the microwave opacity. For the "best" case, there is about twice as much CO_2 microwave opacity as H_2O opacity. The value of M indicates that the sum of the two opacities will be quite significant in reducing the microwave brightness temperature found below 3 cm in wavelength from the value of the surface brightness temperature. For a surface temperature of 700°K, there is so much opacity that all the reduction in the radar cross section between 12.5 and 3.8 cm can be attributed to atmospheric absorption. In fact, for the best model, the M value at 700° K is a factor of 3 too much. We note that M is very sensitive to the choice of a_{CO_2} and T_s. Even for a surface temperature of 543° K, M will range between 1/2 and 2 (it equals 1.5 for the "best" model) and so there will be appreciable microwave opacity below 3 cm in wavelength. We note that part of the decrease in cross section from 12.5 cm to 3.8 cm may be due to a decrease in dielectric constant (Pollack and Sagan, 1965a). An M value of 1 gives a good fit for the microwave spectrum when T_s = 700° K. If T_s is as low as 543° K, the observed brightness temperature would be too low by between 100 and 150° K at long wavelengths, where there is negligible atmospheric attenuation. Clearly, the problem of fitting the microwave spectrum must be reconsidered.

We now summarize the basic results of this section. For all models, the atmosphere is convectively unstable and an adiabatic lapse rate is expected between the clouds and surface in approximate agreement with the spacecraft findings. As a result of the large instability near the surface, it is the solar energy deposited below the clouds and not the amount deposited at the ground that determines the greenhouse effect. If we assume that CO_2 and H_2O vapor are the only source of infrared opacity below the clouds and use the mixing ratio of CO_2 and the pressure found by the spacecraft

experiments, our greenhouse models require amounts of H_2O in the lower atmosphere, which are in reasonable agreement with the amount apparently detected. In addition, cloud-bottom temperatures close to the freezing point of water are found and the H_2O vapor and CO_2 will both be important sources of microwave opacity. Table XII and Figs. 4 through 9 present the greenhouse requirement for various constraints on the CO_2 mixing ratio and cloud-top pressure.

IV. CRITIQUE OF OTHER GREENHOUSE MODELS

The discovery of the high surface temperature on Venus has engendered a large number of models attempting to explain this phenomenon, including the present paper. We briefly review and comment upon these other models.

In 1940, Wildt (1940) considered the effect of the then estimated amount of carbon dioxide in the Venus atmosphere and concluded that it would cause only a very modest greenhouse effect of no more than 50° K. As mentioned above, carbon dioxide has a number of window regions and so, some additional source of opacity, such as water vapor, is needed for a large greenhouse effect.

The first modern greenhouse model was proposed by Sagan (1960). His model employed CO_2 and H_2O vapor opacity to cause the greenhouse effect and he estimated these quantities from boiler-furnace emissivities for each of the gases, with some attempt made to correct for wavelength overlap. Little attempt was made to treat the solar-energy deposition, and the greenhouse constraints were obtained by demanding that there be enough opacity to adequately reduce the radiation flux from the surface at the top of the atmosphere to an amount equal to the deposited solar energy.

Sagan's model was criticized by Jastrow and Rasool (1962), who pointed to the need to carry out a more detailed radiative-transfer calculation. A sample grey calculation indicated that much higher opacities were needed when this was done. Jastrow and Rasool also did little with the solar-energy

deposition problem nor did they attempt to identify their grey opacity requirement with the properties of a specific infrared absorber.

Further work on a gaseous greenhouse model was done by Plass and Wyatt (1962), who showed that at pressures of tens of atm, CO_2 can be quite opaque at most infrared wavelengths. However, their greenhouse model again improperly allowed for atmospheric infrared radiation and so is subject to the same criticism as Sagan's early work. These authors also neglected radiation beyond 20 μ. There is enough radiation at these wavelengths to decrease significantly the greenhouse effect if the proposed absorber does not absorb beyond 20 μ, as is the case for CO_2.

Ohring and Mariano have stressed the role that condensation clouds could play in achieving the greenhouse effect. In one paper (Ohring and Mariano, 1964), they show how clouds that were opaque in the infrared and covered a large fraction of the planet needed only a very modest amount of atmospheric opacity to achieve the required radiation balance. However, they assumed that the atmosphere was nearly adiabatic up to the cloud level. In so doing, they neglected the most important part of a greenhouse calculation. Such lapse rates will pertain only if there is a continuously distributed strong source of infrared opacity below the clouds and this opacity source is evidently the most important contributer to a high surface temperature.

In another cloud model, Ohring et al. (1964) considered an opaque cloud layer extending to the 373° K level, below which opacity was supplied by some grey absorber in radiative equilibrium. Such models are defective in not comparing the grey absorber with some real material and in assuming a priori that radiation equilibrium holds.

A third class of greenhouse models envisions aerosols such as dust particles distributed throughout the atmosphere. One apparently obvious advantage of such a model is that large opacities over the entire infrared domain can be achieved with such solid absorbers. On the other hand, a common problem is that the aerosols might be so opaque even to sunlight that no

sunlight will reach the ground. It must be remembered that these aerosols will be quite small if they are to stay aloft for any length of time, and so it is not obvious a priori that such particles will be opaque at all infrared wavelengths. Naturally, scattering will abet the absorption process, but it is still of great interest for the absorption properties of common materials to be determined. It might be pointed out that below 5 μ in wavelength, Al_2O_3, calcite, and quartz particles of small dimension ($\sim$10 μ) are fairly transparent (Gray, 1963).

The first such dust model was proposed by Öpik (1961). He assumed a priori that all the solar energy would be deposited at the top of the atmosphere and invoked wind friction as a means of supplying heat to the surface. To keep the aerosols aloft, he required the atmosphere to be in convective equilibrium. One objection to Öpik's model, although not a fundamental one to dust models per se, is that with a convective atmosphere the solar flux deposited at the top will be transferred to the ground chiefly by convection and there is no need to invoke a minor heat-input mechanism like wind friction. If all the solar energy is deposited at the top, then the infrared net flux below this level will be zero and for a local theory the atmosphere will be isothermal. In this sense, Öpik's model is self-contradictory.

Goody and Robinson (1966) attempted to circumvent this latter difficulty by having global circulation play a role and be the causative agent of an adiabatic lapse rate below the clouds. Analogy was drawn to the situation for terrestrial oceans. Again the sunlight was assumed a priori to be deposited in one narrow region of the atmosphere. While such a model pertains most reasonably to a dust layer, the authors also considered its application to a water-cloud layer extending to the surface of the planet. Even without the Soviet results, this specific model is clearly inapplicable to Venus since a microwave opacity of more than 10^4 of the observed value would thereby be engendered (Pollack and Sagan, 1967b). A more fundamental criticism has come from Hess (1967), whose calculations indicated that global circulation would not lead to a substantial adiabatic layer below the level of deposition. In addition, as we will mention immediately below, the solar energy is not absorbed in a thin layer of the atmosphere.

Samuelson (1967) has made a major contribution to the dust model by explicitly calculating the solar-energy deposition from single-scattering albedos implied by the visual reflectivity of Venus. These single-scattering albedos are quite high and so solar energy penetrates fairly deeply into the dust layer and is not localized in one place. Samuelson overestimated the greenhouse effect by assuming the dust layer was infinitely deep and in radiative equilibrium. While his asymptotic temperatures were too low to be compatible with the radio-derived average surface temperature of 700° K, they may not be in very severe disagreement with the Venera 4 value of 550° K. Furthermore, Samuelson did not realize that the visual, single-scattering albedo of the dust particle, which was derived by Sobolev (1963) from the observed reflectivity, is very sensitive to the choice of phase function. While Sobolev tried to derive the phase function, his theory is a gross approximation. A more forward-scattering phase function than the one employed by Sobolev implies a higher single-scattering albedo and hence a larger greenhouse effect. Samuelson's work can be improved upon both in this way and by allowing for convective instability.

Finally, Hansen and Matsushima (1967) supposed that solar energy cannot reach the surface and added an additional heat source in the form of the sub-surface heat flux due to radioactive heating. While this heat flux was several orders of magnitude smaller than the solar-heat flux, they obtained the required hot surface by increasing the aerosol opacity sufficiently. Although the equilibrium form of this model is reasonable, it is unclear how the atmosphere evolved to the equilibrium state: Once there is so much dust that sunlight could not penetrate to the surface, it is hard to see how additional dust could be added.

ACKNOWLEDGMENTS

I am especially indebted to Carl Sagan for interesting me in the greenhouse problem and for useful discussions of this paper. I am also grateful to Mr. David Ziskind of the SAO computer center for programming parts of the greenhouse calculations and to Mrs. Elinore Green for assisting with other calculations and for preparing the initial graphs. This investigation was supported in part by NASA grant NGR-09-015-023.

REFERENCES

Barath, F. T., Barrett, A. H., Copeland, J., Jones, D. E., and Lilley, A. E. (1964). Mariner 2 microwave experiment and results. Astron. J., 69, 49-58.

Barrett, A. H., and Staelin, D. H. (1964). Radio observations of Venus and the interpretations. Space Sci. Rev. 3, 109-135.

Belton, M. J., and Hunten, D. M. (1967). Report to the Tucson Conference on the atmospheres of Venus and Mars.

Blanco, V. M., and McCuskey, S. W. (1961). "Basic Physics of the Solar System." Addison-Wesley Publ. Co., Reading, Mass., 307 pp.

Burch, D. E., and Gryvnak, D. A. (1966). Absorption by H_2O between 5045-14,485 cm^{-1}. Aeronutronic Publication No. U-3704.

Burch, D. E., Gryvnak, D. A., and Paty, R. R. (1965). Absorption by CO_2 between 8000 and 10,000 cm^{-1}. Aeronutronic Publication No. U-3200.

Burch, D. E., Gryvnak, D. A., and Williams, D. (1966). Infrared absorption by carbon dioxide. Ohio State Univ. Report No. 778.

Chamberlain, J. W. (1965). The atmosphere of Venus near her cloud tops. Astrophys. J. 141, 1184-1205.

Clark, B. G., and Kuz'min, A. D. (1965). The measurement of the polarization and brightness distribution of Venus at 10.6 cm wavelength. Astrophys. J. 142, 23-44.

Connes, P., Connes, J., Benedict, W. S., and Kaplan, L. D. (1967). Traces of HCl and HF in the atmosphere of Venus. Astrophys. J. 147, 1230-1237.

Davis, P. A., and Viezie, W. (1964). A model for computing infrared transmission through atmospheric water vapor and carbon dioxide. J. Geophys. Res. 69, 3785-3794.

Evans, D. C., Boggess, A., III, and Scolnik, R. (1965). The reflectivity of Venus and Jupiter in the middle ultraviolet. Astron. J. 70, 321.

Goody, R. M., and Robinson, A. R. (1966). A discussion of the deep circulation of the atmosphere of Venus. Astrophys. J. 146, 339-355.

Gray, D. E., ed., (1963) "American Institute of Physics Handbook." McGraw-Hill, New York.

Hansen, J. E., and Matsushima, S. (1967). The atmosphere and surface temperature of Venus: A dust insulation model. Astrophys. J. 150, 1139-1157.

Hess, S. L. (1959). "Introduction to Theoretical Meteorology." Henry Holt, New York.

Hess, S. L. (1967). In preparation.

Ho, W., Kaufman, I. A., and Thaddeus, P. (1966). Laboratory measurement of microwave absorption models of the atmosphere of Venus. J. Geophys. Res. 71, 5091-5107.

Howard, T. N., Burch, D. E., and Williams, D. (1956). Infrared transmission of synthetic atmospheres. J. Opt. Soc. Am. 46, 186-190, 237-245, 334-338, 452-455.

Irvine, W. M., and Pollack, J. B. (1968). Infrared optical properties of water and ice spheres. Icarus, in preparation.

Jastrow, R., and Rasool, S. I. (1963). Radiative transfer in the atmosphere of Venus and Mars. In "Space Research III, Proceedings of the COSPAR Symposium." (W. Priester, ed.), North-Holland Press, Amsterdam, 1036-1041.

Karp, D., Morrow, W. E., Jr., and Smith, W. B. (1964). Radar observations of Venus at 3.6 centimeters. Icarus, 3, 473-475.

Kliore, A., Levy, G. S., Cain, D. L., Fjelbo, G., and Rasool, S. I. (1967). Atmosphere and ionosphere of Venus from the Mariner V S-band radio occultation measurement. Science 158, 1683-1688.

Low, F. J. (1965). Planetary radiation at infrared and millimeter wavelengths. Lowell Obs. Bulletin No. 128, VI, 184-187.

Moroz, V. I. (1963). The infrared spectrum of Venus (1-1.25 μ) Am. Transl.-Sov. Astron. J. 7, 109-115.

Nature (1967). More News from Venus, 216, 427-428.

Ohring, G., Brooks, E. M., and Mariano, J. (1964). The meteorology of Mars and Venus. Geophys. Corp. of Am. Tech. Rep. No. 64-4-N.

Ohring, G., and Mariano, J. (1964). The effect of cloudiness on a greenhouse model of the Venus atmosphere. J. Geophys. Res. 69, 165-175.

Öpik, E. J. (1961). The aeolosphere and atmosphere of Venus. J. Geophys. Res. 66, 2807-2819.

Palmer, C. H., Jr. (1960). Experimental transmission functions for the pure rotation band of water vapor. J. Opt. Soc. Am. 50, 1232-1242.

Plass, G. N., and Wyatt, V. R. (1962). Carbon dioxide absorption for path lengths applicable to the atmosphere of Venus. Aeronutronic Publication No. U-1844.

Pravda, 1967a, Oct. 24.

Pravda, 1967b, Nov. 1.

Pollack, J. B. (1968). Temperature structure of nongrey planetary atmospheres. Icarus, in preparation.

Pollack, J. B., and Sagan, C. (1965a). The microwave phase effect of Venus. Icarus 4, 62-103.

Pollack, J. B., and Sagan, C. (1965b). The infrared limb darkening of Venus. J. Geophys. Res. 70, 4403-4425.

Pollack, J. B., and Sagan, C. (1967a). A critical test of the electrical discharge model of the Venus microwave emission. Astrophys. J. 150, 699-709.

Pollack, J. B., and Sagan, C. (1967b). An analysis of the Mariner 2 microwave observations of Venus. Astrophys. J. 150, 327-344.

Pollack, J. B., and Sagan, C. (1968). A discussion of the paper by D. G. Rea and B. T. O'Leary. "On the composition of the Venus clouds." J. Geophys. Res., in preparation.

Sagan, C. (1960). The radiation balance of Venus. J. P. L. Tech. Rep. No. 32-34.

Sagan, C. (1967). An estimate of the surface temperature of Venus independent of passive microwave radiometry. Astrophys. J. 149, 731-733.

Sagan, C. (1968). A comparison of grey and nongrey atmospheres. Icarus, to be published.

Sagan, C., and Pollack, J. B. (1967). Anisotropic nonconservative scattering and the clouds of Venus. J. Geophys. Res. 72, 469-477.

Sagan, C., and Pollack, J. B. (1968). On the structure of the Venus atmosphere. In preparation.

Samuelson, R. E. (1967). Greenhouse effect in semi-infinite scattering atmospheres: Application to Venus. Astrophys. J. 147, 782-798.

Sinton, W. M. (1963). Infrared observation of Venus. In "Proceedings of the Eleventh International Astrophysical Symposium, The Physics of Planets." University of Liège, Belgium, 300-310.

Sinton, W. M., and Strong, J. (1960). Radiometric observations of Venus, Astrophys. J. 131, 470-490.

Sobolev, V. V. (1963). "A Treatise on Radiative Transfer." D. Van Nostrand Co., Princeton, N. J., 319 pp.

Solomon, P. (1966). Private communication.

Stauffer, F. R., and Walsh, T. E. (1966). Transmittance of water vapor — 14 to 20 microns. J. Opt. Soc. Am. 56, 401-405.

Stull, V. R., Wyatt, P. J., Plass, G. N. (1963). The infrared absorption of carbon dioxide. Aeronutronic Rep. No. SSD-TDR-62-127, III.

Walker, R. (1966). Infrared Photometry of Stars and Planets. Harvard Ph. D. thesis.

Walker, R., and Sagan, C. (1966). The ionospheric model of the Venus microwave emission: an obituary. Icarus 5, 105-123.

Wildt, R. (1940). Note on the surface temperature of Venus. Astrophys. J. 91, 266-268.

Wyatt, P. J., Stull, V. R., and Plass, G. N. (1962). Infrared absorption of water vapor. Aeronutronic Rep. No. SSD-TDR-62-127, II.

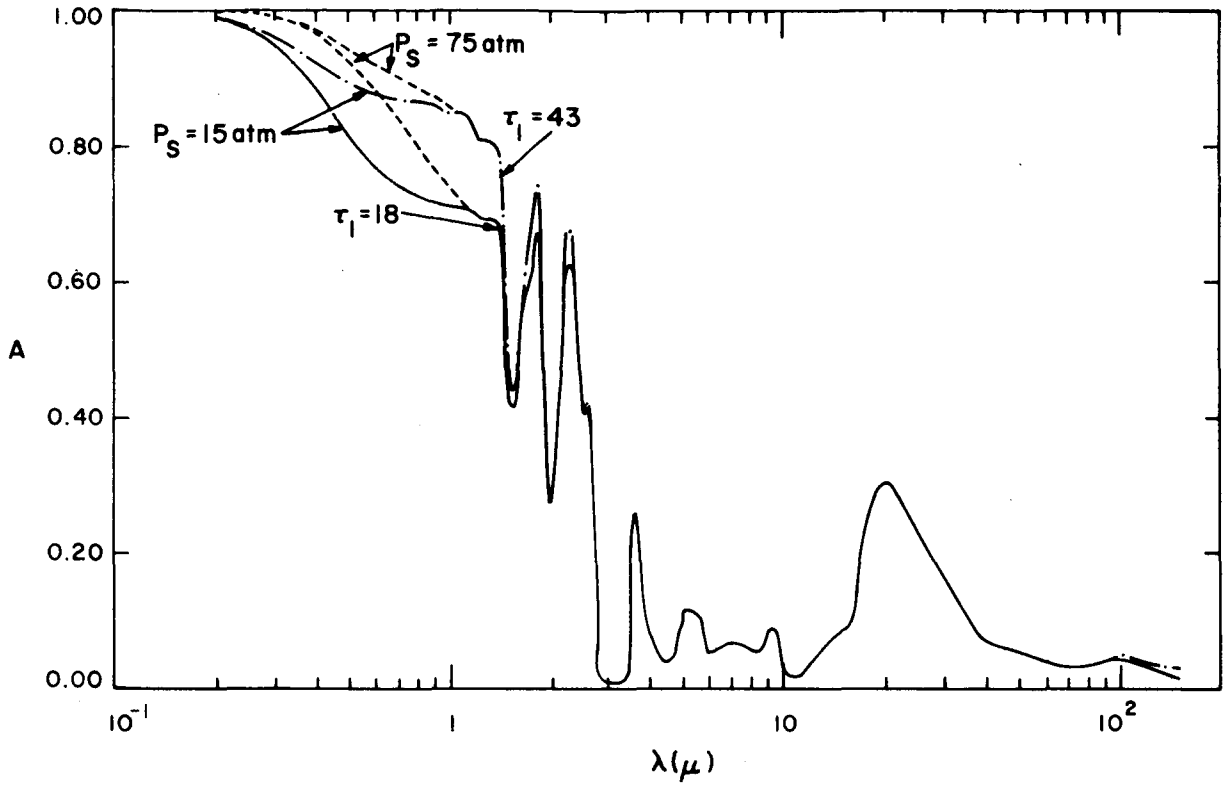

Fig. 1. Spherical albedo A as a function of wavelength λ, in units of microns. The calculations pertain to scattering by the clouds and atmosphere, but neglect gaseous absorption. The ice-cloud particles have an average radius of 7.5 μ. The calculations were performed for two surfact pressures P_s, and two cloud optical thicknesses τ_1. The atmosphere was assumed to be composed primarily of nitrogen. For atmospheres composed primarily of carbon dioxide, the indicated surface pressure should be divided by 1.55.

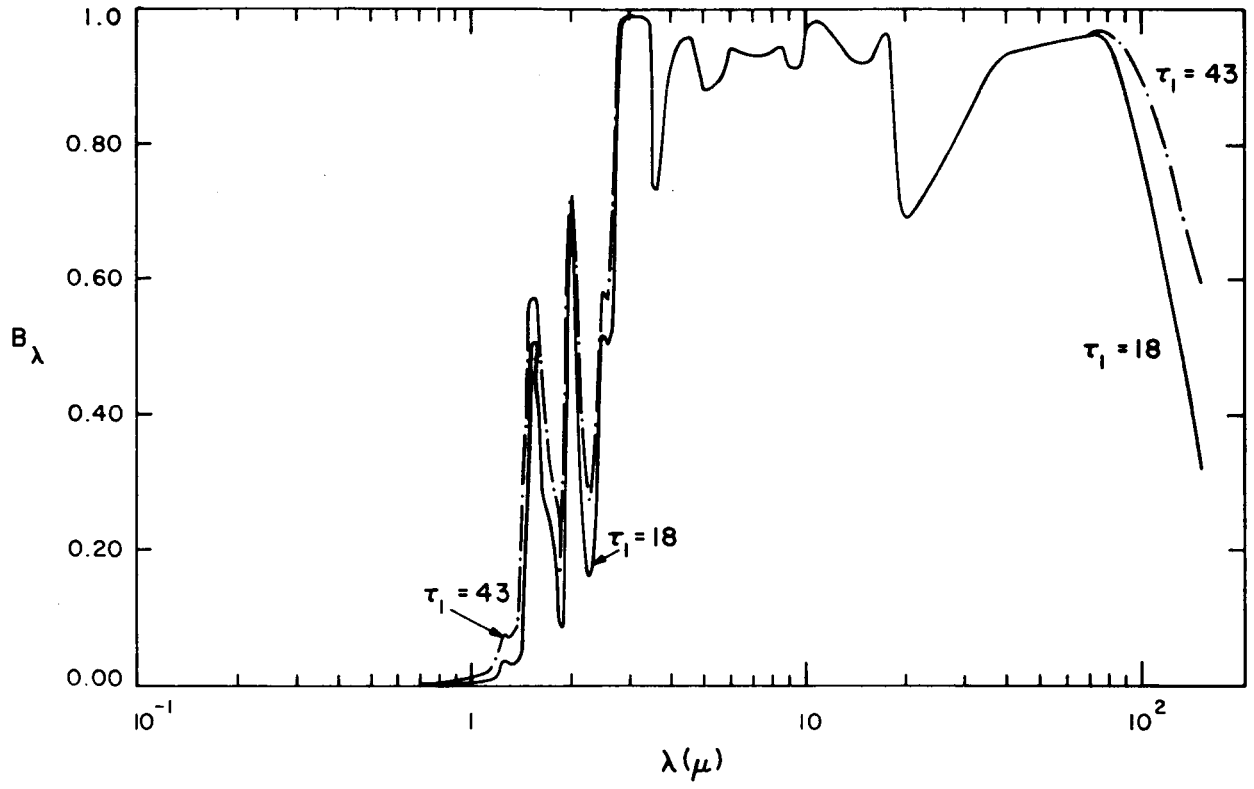

Fig. 2. Absorptivity B, of an ice cloud as a function of wavelength λ, in units of microns. The cloud particles have an average radius of 7.5 μ and several optical depths τ_1 are employed.

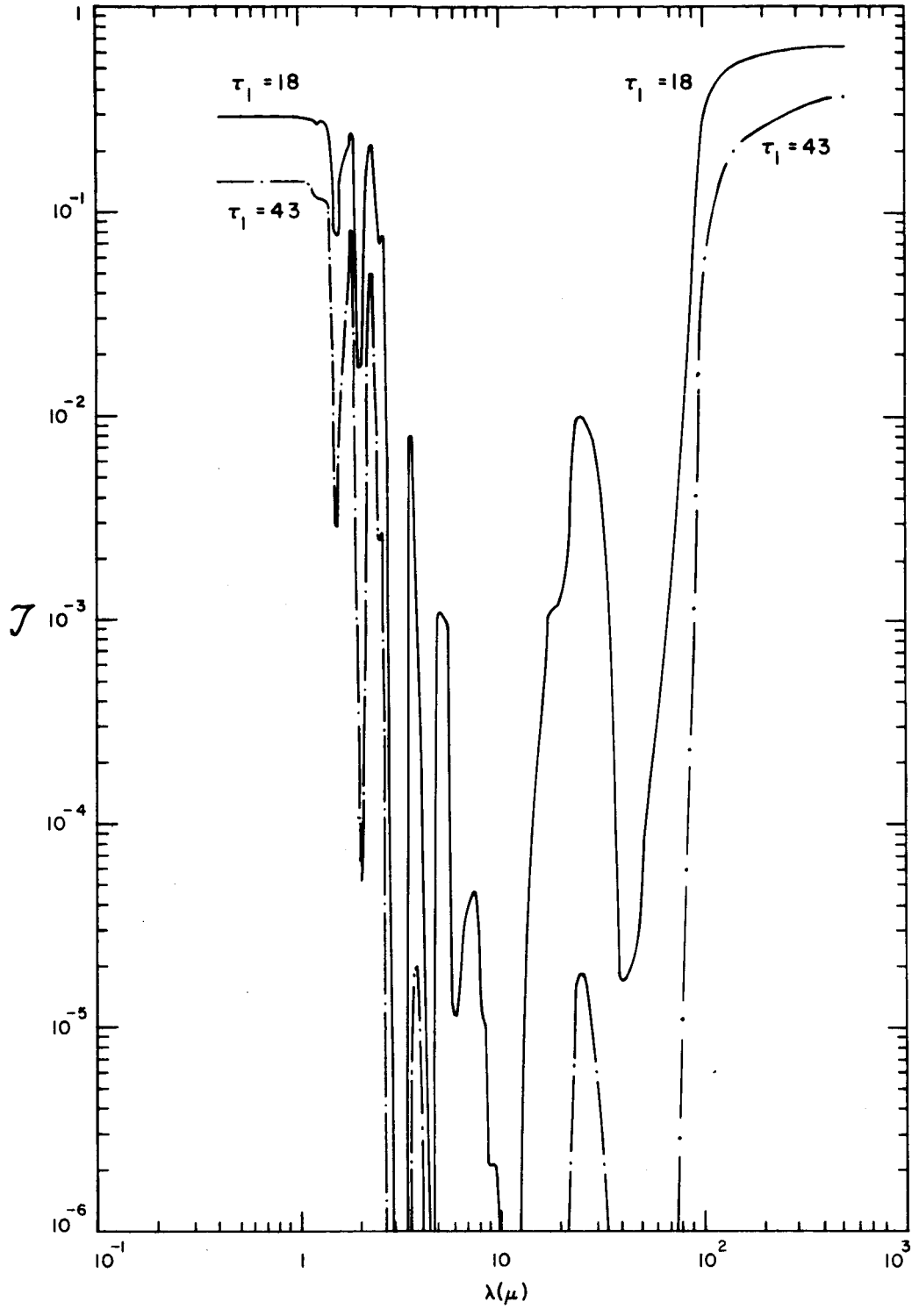

Fig. 3. Transmissivity $\mathcal{T}$, of an ice cloud as a function of wavelength λ, in units of microns. The cloud particles have an average radius of 7.5 μ and several optical depths τ_1 are employed.

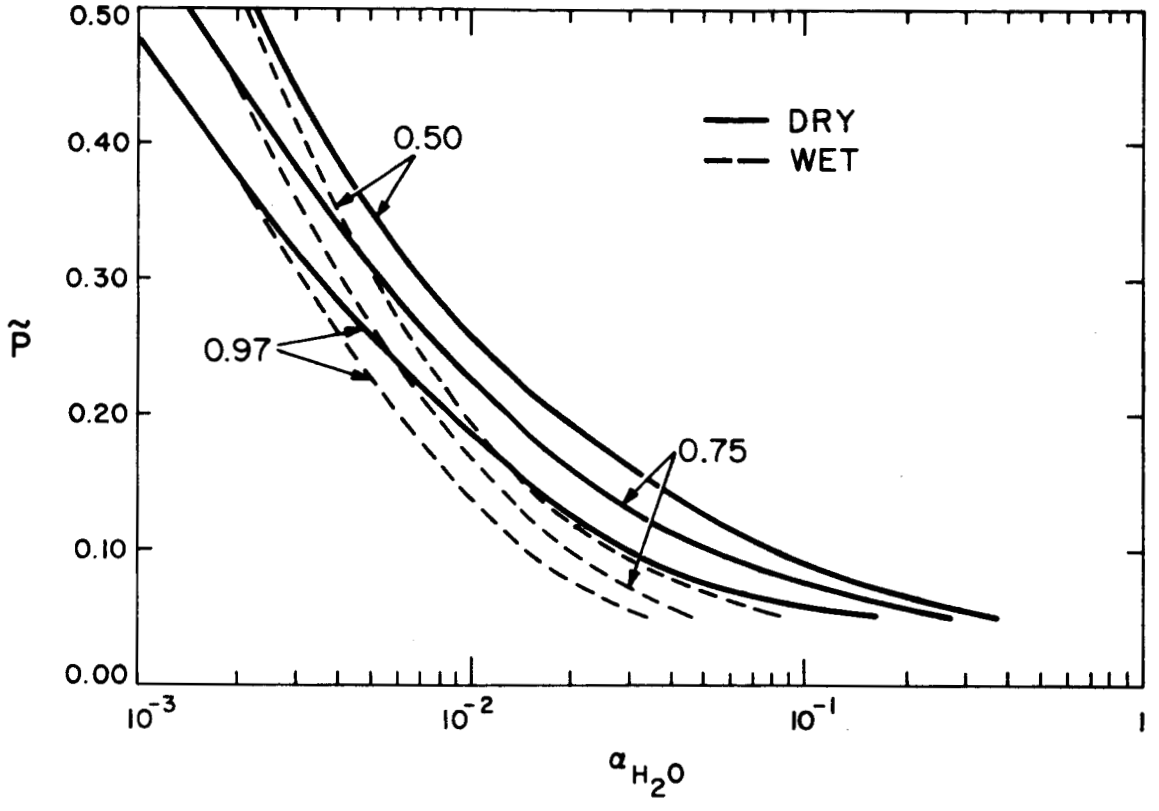

Fig. 4. The water-vapor mixing ratio a_{H_2O}, required for the desired greenhouse effect as a function of the cloud-top pressure $\tilde{P}$. The carbon dioxide mixing ratio assumed in the calculation of a given curve is indicated. Solid lines correspond to a model with an assumed dry adiabatic lapse rate within the clouds, while the dashed lines correspond to a wet adiabat within the clouds.

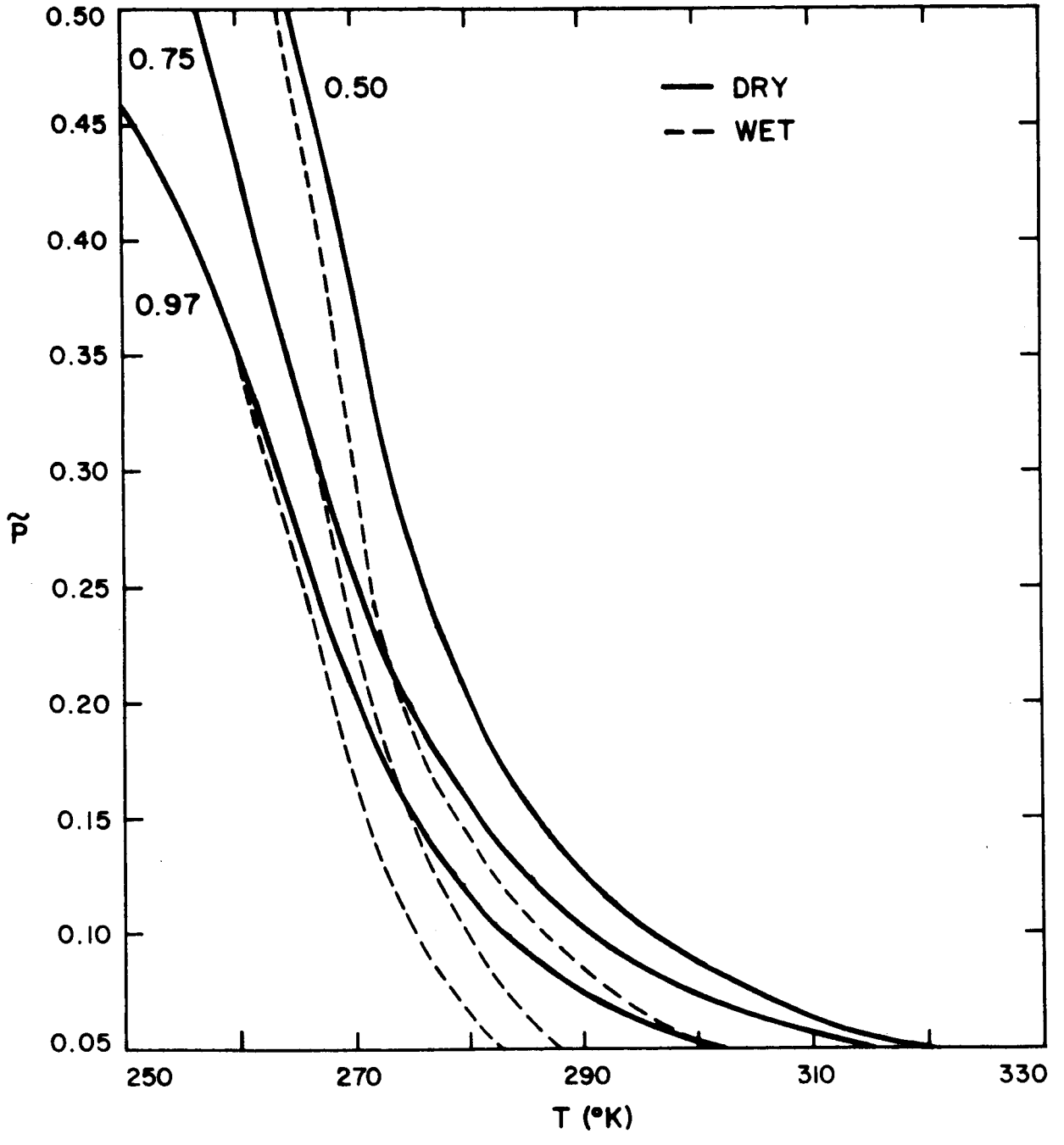

Fig. 5. The cloud-bottom temperature T, as a function of the cloud-top pressure $\tilde{P}$, for various successful greenhouse models. The carbon dioxide mixing ratio assumed in the calculation of a given curve is indicated. Solid lines correspond to a model with an assumed dry adiabatic lapse rate within the clouds, while the dashed lines correspond to a wet adiabat within the clouds.

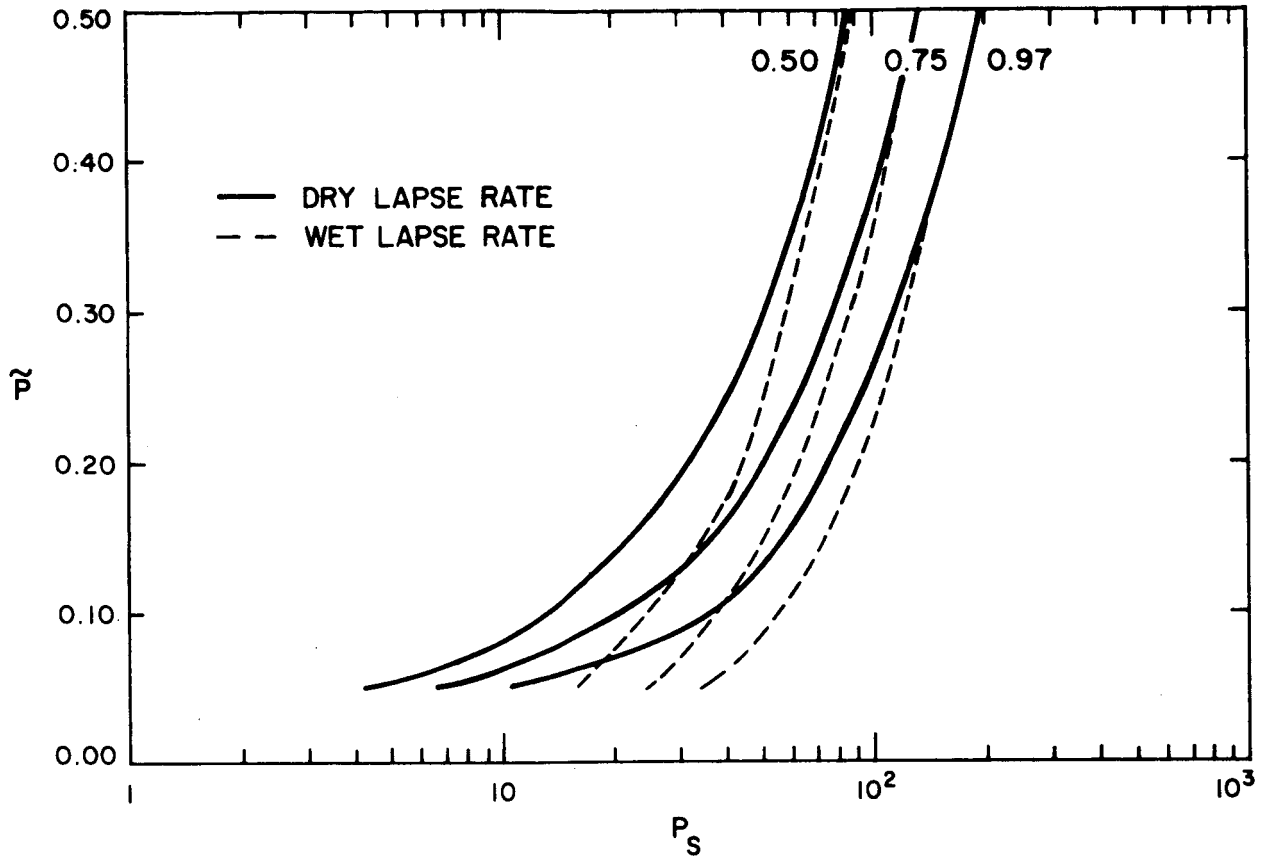

Fig. 6. Surface pressure P_s, as a function of the cloud-top pressure $\tilde{P}$, for various successful greenhouse models. A surface temperature of 700° K was assumed. The carbon dioxide mixing ratio assumed in the calculation of a given curve is indicated. Solid lines correspond to a model with an assumed dry adiabatic lapse rate within the clouds, while the dashed lines correspond to a wet adiabat within the clouds.

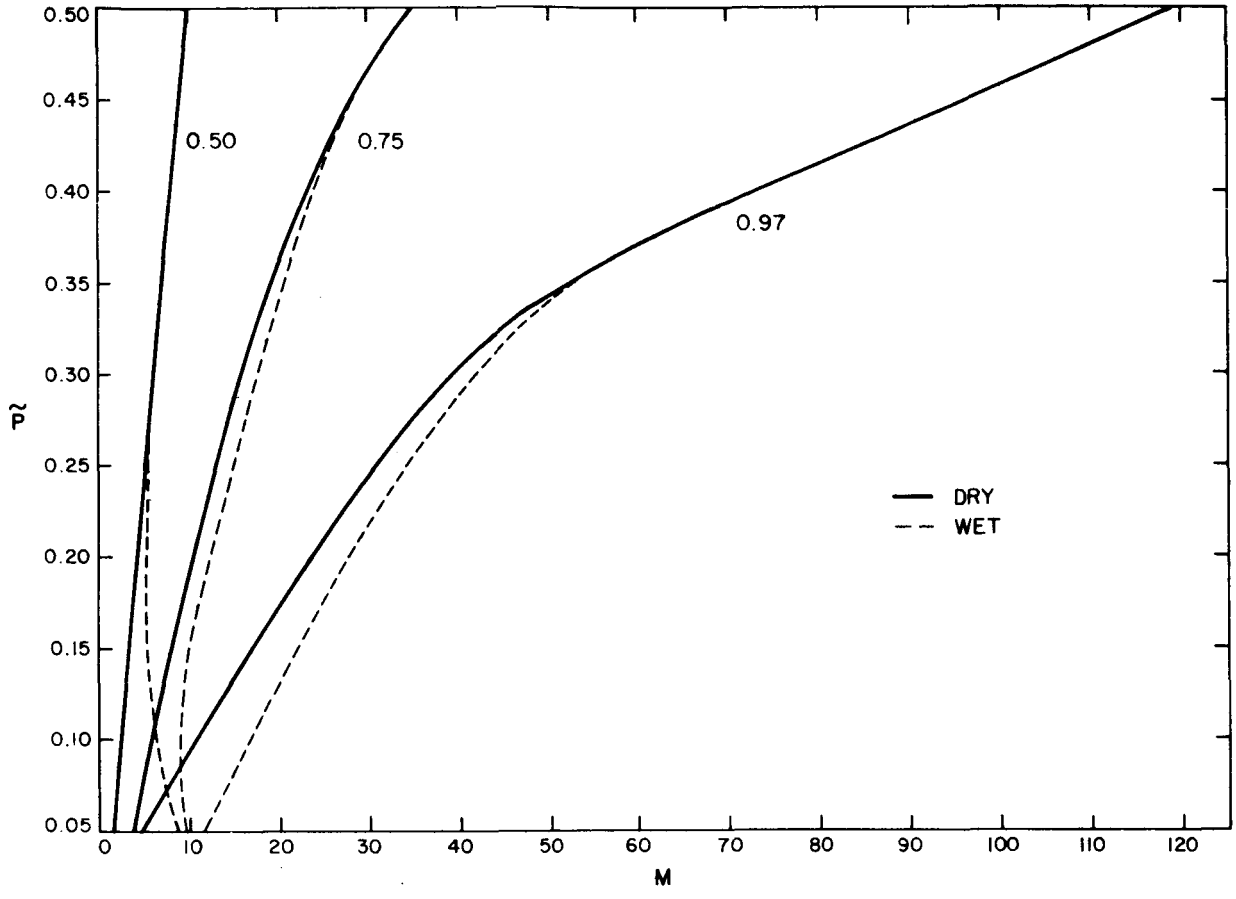

Fig. 7. Microwave parameter M, as a function of the cloud-top pressure $\tilde{P}$, for various successful greenhouse models; M is the ratio of the actual opacity for an assumed surface temperature of 700° K to that required by the Ho et al. best fit to the passive microwave data. The carbon dioxide mixing ratio assumed in the calculation of a given curve is indicated. Solid lines correspond to a model with an assumed dry adiabatic lapse rate within the clouds, while the dashed lines correspond to a wet adiabat within the clouds.

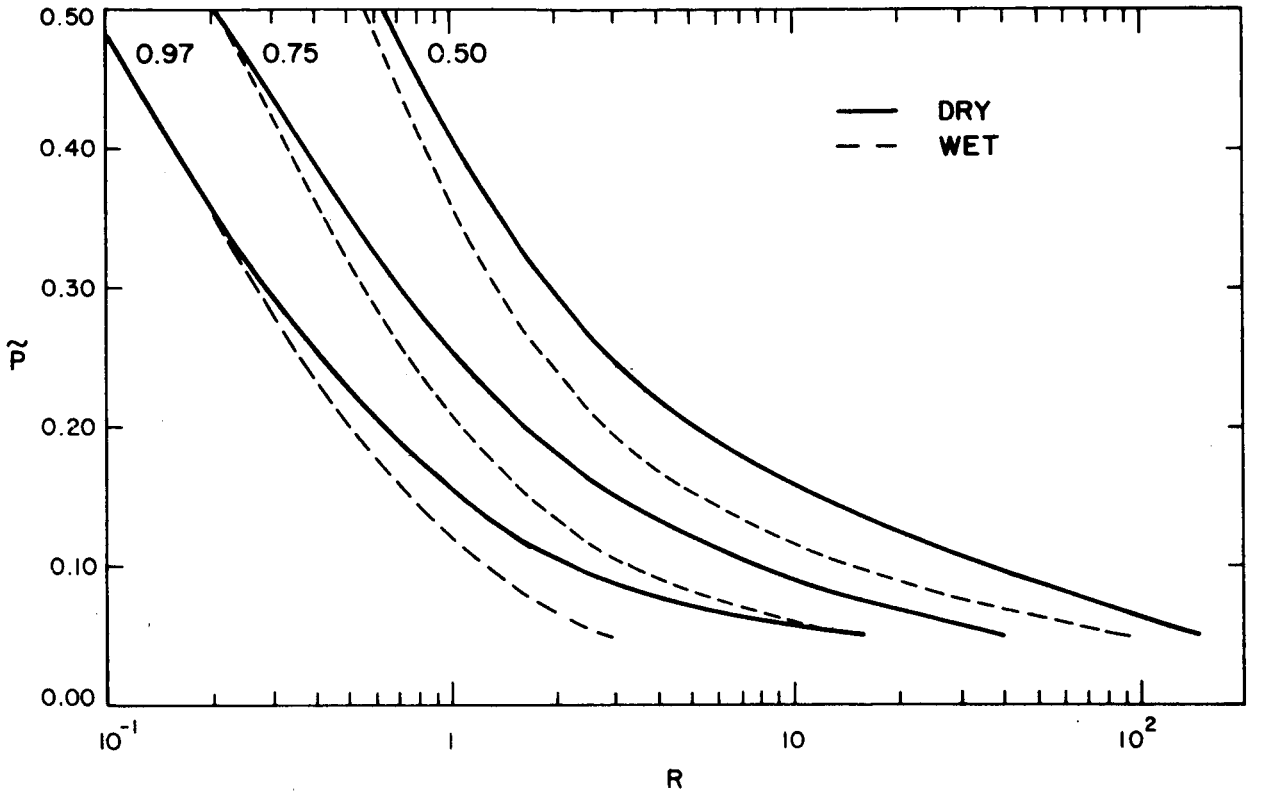

Fig. 8. Microwave parameter R as a function of the cloud-top pressure $\tilde{P}$ for various successful greenhouse models; R is the ratio of the microwave opacity due to water vapor to that due to carbon dioxide and nitrogen. The carbon dioxide mixing ratio assumed in the calculation of a given curve is indicated. Solid lines correspond to a model with an assumed dry adiabatic lapse rate within the clouds, while the dashed lines correspond to a wet adiabat within the clouds.

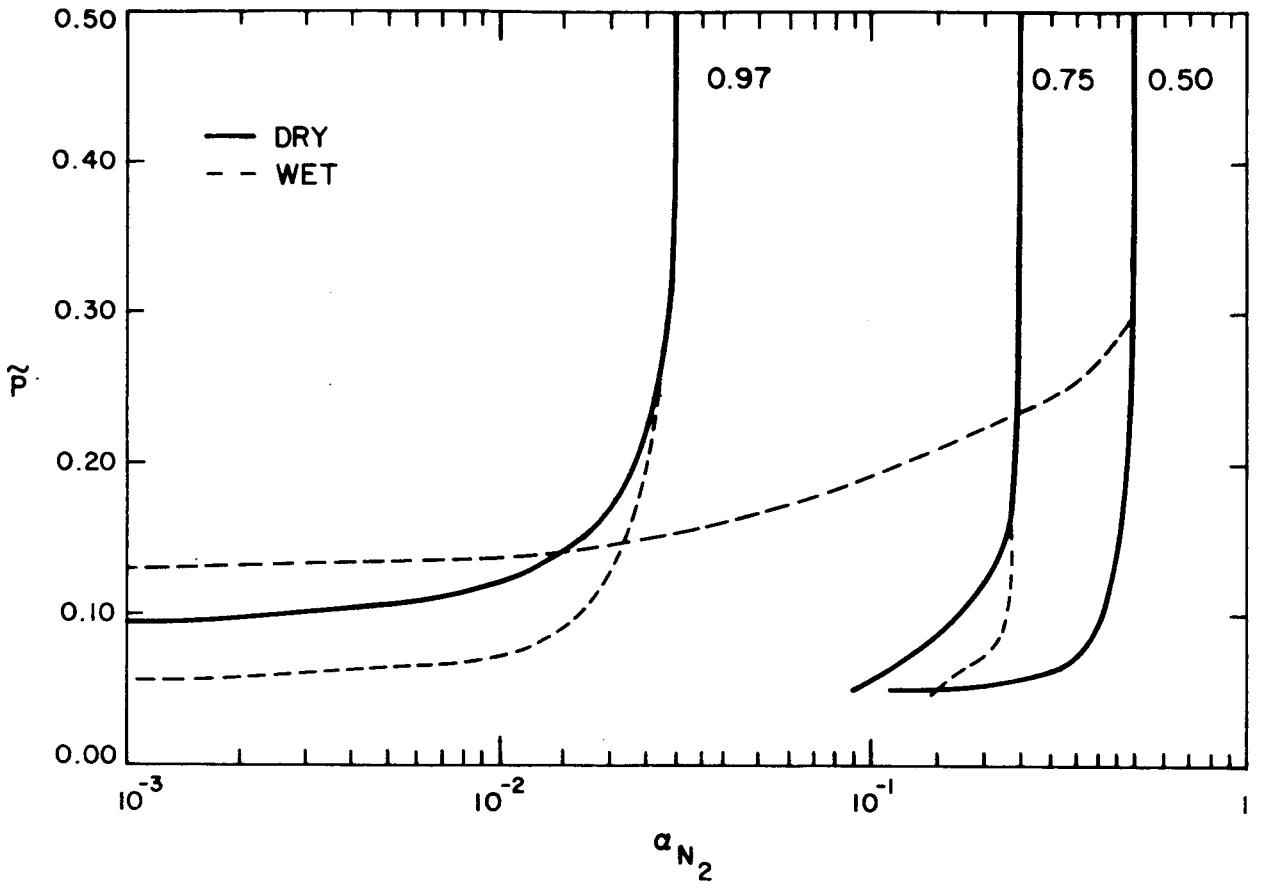

Fig. 9. Nitrogen mixing ratio a_{N_2} as a function of the cloud-top pressure $\tilde{P}$ for various successful greenhouse models. The parameter a_{N_2} is calculated by assuming that nitrogen, carbon dioxide, and water vapor are the major constituents of the Venus atmosphere. The carbon dioxide mixing ratio assumed in the calculation of a given curve is indicated. Solid lines correspond to a model with an assumed dry adiabatic lapse rate within the clouds, while the dashed lines correspond to a wet adiabat within the clouds.

TABLE I

Values of the Equivalent-Width Parameters

Band Center		Limits							
(μ)	(cm^{-1})	(cm^{-1})	c	d	k	$\Delta\nu_\ell$ (cm^{-1})	C	D	K
				CO_2					
14.8	675	550- 800	5.21	0.50	0.43	50	-58	55	47
4.29	2330	2160- 2500	22.0	0.54	0.50	50	+ 27.5	34	31.5
2.75	3640	3480- 3800	4.65	0.58	0.51	50	-137	77	68
2.01	4975	4750- 5200	0.469	0.50	0.41	80	-536	138	114
1.59	6275	6000- 6550	0.063	0.50	0.38	80	-637	119	90
1.44	6950	6650- 7250	0.058	0.50	0.41	80	-736	130	107
1.22	8162	8000- 8325	0.0133	0.50	0.41	80	-453	70.5	58
1.06	9475	9300- 9650	0.00182	0.50	0.41	80	-626	76.0	62
				H_2O					
6.25	1600	1150- 2050	339	0.50	0.36	160	+302	218	157
3.26	3370	2800- 3340	40.2	0.50	0.30	500	+447	134	80.4
2.58	3870	3340- 4400	380	0.50	0.30	200	+337	246	150
1.87	5350	4800- 5900	132	0.50	0.31	275	+127	232	144
1.38	7250	6500- 8000	242	0.50	0.22	350	+202	460	198
1.14	8800	8300- 9300	31	0.50	0.26	350	-172	248	129
0.926	10800	10100-11500	38	0.50	0.27	350	-311	347	187
0.813	12300	11800-12800	6.86	0.50	0.27	350	-497	248	134
0.719	13900	13400-14400	7.23	0.50	0.27	350	-486	248	134

TABLE II

Window Regions at the Bottom of the Atmosphere

P_s = 15 atm		P_s = 300 atm	
Gas mixture B (μ)	Gas mixture A (μ)	Gas mixture B (μ)	Gas mixture A (μ)
0.400-0.711	0.400-0.705	0.400-0.699	0.400-0.692
0.728-0.803	0.735-0.794	0.741-0.787	0.749-0.779
0.823-0.892	0.833-0.878	0.841-0.865	0.850-0.852
0.963-1.055	0.980-1.050	0.996-1.049	1.015-1.040
1.056-1.097	1.061-1.082	1.062-1.069	
1.178-1.220	1.196-1.209		
1.231-1.248			
1.541-1.565			
1.623-1.715	1.655-1.680		
2.117-2.235			

TABLE III

Deposition of Solar Energy Among Various Sinks

	P = 15 atm				P = 75 atm				P = 300 atm			
	$\tau_1 = 18$		$\tau_1 = 43$		$\tau_1 = 18$		$\tau_1 = 43$		$\tau_1 = 18$		$\tau_1 = 43$	
	A	B	A	B	A	B	A	B	A	B	A	B
n(a)	0.329	0.258	0.430	0.373	0.484	0.406	0.522	0.469	0.601	0.550	0.596	0.545
n(c)	0.0760	0.1024	0.0857	0.1140	0.0912	0.1250	0.0924	0.1222	0.1036	0.1385	0.0986	0.1315
n(g)	0.437	0.474	0.272	0.290	0.240	0.269	0.1595	0.1715	0.0905	0.0994	0.0685	0.0744
n(x)	0.1577	0.1650	0.212	0.222	0.1866	0.1985	0.227	0.237	0.203	0.212	0.237	0.250
n′(c)	0.1289	0.1495	0.271	0.307	0.1539	0.1816	0.291	0.328	0.1718	0.1990	0.306	0.349
n′(a)	0.0862	0.0332	0.1172	0.0454	0.1020	0.0400	0.1254	0.0484	0.1112	0.0427	0.1311	0.0511
n″(a)	0.1898	0.1776	0.1268	0.1348	0.319	0.309	0.1978	0.215	0.422	0.447	0.258	0.277

TABLE IV

Energy Deposition Profile*

	P = 15 atm				P = 75 atm				P = 300 atm			
	τ_1 = 18		τ_1 = 43		τ_1 = 18		τ_1 = 43		τ_1 = 18		τ_1 = 43	
	A	B	A	B	A	B	A	B	A	B	A	B
Δh(1)	0.770	0.243	1.038	0.328	0.910	0.292	1.110	0.350	0.992	0.312	1.160	0.369
Δh(2)	0.391	0.1636	0.528	0.223	0.463	0.1969	0.565	0.238	0.504	0.210	0.590	0.251
Δh(3)	0.295	0.1316	0.401	0.1783	0.349	0.1584	0.428	0.1901	0.380	0.1692	0.448	0.2005
Δh(4)	0.262	0.1214	0.356	0.1669	0.310	0.1461	0.381	0.1780	0.338	0.1560	0.398	0.1877
Δh(5)	0.438	0.1709	0.607	0.239	0.518	0.206	0.650	0.254	0.565	0.220	0.680	0.268
Δh(7)	0.0458	0.0481	0.0299	0.0315	0.0542	0.0579	0.0320	0.0336	0.0591	0.0618	0.0335	0.0354
Δh(8)	0.01533	0.01526	0.01344	0.01388	0.01813	0.01837	0.01437	0.01478	0.01975	0.01963	0.01502	0.01560
Δh(9)	7.90×10^{-3}	7.92×10^{-3}	5.22×10^{-3}	5.80×10^{-3}	9.34×10^{-3}	9.53×10^{-3}	5.58×10^{-3}	6.18×10^{-3}	0.01018	0.01019	5.83×10^{-3}	6.52×10^{-3}
Δh(10)	5.45×10^{-3}	2.27×10^{-3}	3.04×10^{-3}	3.32×10^{-3}	6.45×10^{-3}	2.73×10^{-3}	3.26×10^{-3}	3.54×10^{-3}	7.02×10^{-3}	2.92×10^{-3}	3.40×10^{-3}	3.74×10^{-3}
Δh(11)					2.84×10^{-3}	4.52×10^{-3}	1.905×10^{-3}	1.898×10^{-3}	3.10×10^{-3}	4.82×10^{-3}	1.991×10^{-3}	2.002×10^{-3}
Δh(12)					1.154×10^{-3}	6.20×10^{-4}	7.46×10^{-4}	9.57×10^{-4}	1.257×10^{-3}	6.62×10^{-4}	7.79×10^{-4}	1.009×10^{-3}
Δh(13)									3.32×10^{-4}	5.16×10^{-4}	2.27×10^{-4}	2.21×10^{-4}

*Levels

1 0 atm to 0.04 atm
2 0.04 atm to 0.08 atm
3 0.08 atm to 0.12 atm
4 0.12 atm to 0.16 atm
5 0.16 atm to 0.20 atm
7 cloud bottom to 2 atm
8 2 atm to 5 atm
9 5 atm to 10 atm
10 10 atm to 15 atm
11 15 atm to 30 atm
12 30 atm to 75 atm
13 75 atm to 300 atm

TABLE V

Bolometric Albedo and Effective Temperature

	A_{bol}			
	$\tau_1 = 18$, A	$\tau_1 = 18$, B	$\tau_1 = 43$, A	$\tau_1 = 43$, B
P = 15 atm	0.690	0.704	0.769	0.780
P = 75 atm	0.738	0.754	0.784	0.784
P = 300 atm	0.759	0.769	0.794	0.804
	T_{eff}(°K)			
	$\tau_1 = 18$, A	$\tau_1 = 18$, B	$\tau_1 = 43$, A	$\tau_1 = 43$, B
P = 15 atm	245	242	228	225
P = 75 atm	232	232	224	221
P = 300 atm	230	228	221	218

TABLE VI

Parameters for the Broadband Opacity of CO_2

	Wavelength interval (μ)	r	r′	s	s′	c	c′	W_c	W_c'
4	12.90-17.39	0.331	0.312	0.235	0.205	3.63×10^{-1}	4.73×10^{-1}	6.50	3.10
5	8.89-12.90	0.610	—	0.358	—	2.87×10^{-3}	—	7.73×10^{3}	—
6	7.55- 8.89	0.856	0.816	0.863	0.783	1.29×10^{-6}	2.68×10^{-6}	4.80×10^{6}	4.13×10^{6}
7	5.63- 7.55	0.737	0.702	0.769	0.697	7.97×10^{-6}	1.53×10^{-5}	4.81×10^{6}	4.11×10^{6}
8	4.82- 5.63	0.584	0.405	0.330	0.462	2.05×10^{-3}	1.06×10^{-2}	2.05×10^{4}	2.80×10^{4}
9	3.88- 4.82	0.331	0.508	0.322	0.270	1.29×10^{-1}	3.80×10^{-2}	1.48×10^{2}	2.77×10^{2}
10	3.42- 3.88	0.561	—	0.570	—	1.19×10^{-3}	—	7.99×10^{4}	—
11	2.92- 3.42	0.739	0.799	0.714	—	2.18×10^{-5}	1.08×10^{-5}	1.20×10^{6}	1.00×10^{6}
12	2.58- 2.92	0.230	0.292	0.172	0.149	2.43×10^{-1}	1.55×10^{-1}	—	1.53×10^{2}
13	2.09- 2.58	0.380	0.558	0.368	0.314	1.73×10^{-3}	1.77×10^{-4}	1.89×10^{7}	2.60×10^{6}

TABLE VII

Parameters for the Broadband Opacity of H_2O

	Wavelength interval (μ)	r	r′	s	s′	c	c′	W_c	W_c'
1	50-100	0.497*	0.576*	0.540*	0.450*	28.92	52.75	5.17×10^{-4}	5.17×10^{-4}
2	29.41-50	0.497	0.576	0.540	0.450	18.35	5.35	1.29×10^{-3}	2.75×10^{-3}
3	17.39-29.41	0.562	—	0.427	0.360	4.64	—	3.23×10^{-2}	—
4	12.90-17.39	0.439	—	0.307	0.237	1.59	—	1.42×10^{-1}	—
5	8.89-12.90	0.859	—	0.859	—	0.143	—	6.70	—
6	7.55- 8.89	0.561	0.572	0.464	0.453	0.365	0.362	2.98	2.97
7	5.63- 7.55	0.494	0.352	0.414	0.447	5.78	3.77	1.30×10^{-2}	7.51×10^{-3}
8	4.82- 5.63	0.482	0.424	0.405	0.427	2.19	1.995	8.69×10^{-2}	7.76×10^{-2}
9	3.88- 4.82	0.608	0.667	0.542	0.500	0.132	0.113	14.60	14.51
10	3.42- 3.88	0.789	0.765	0.556	0.515	0.0799	0.0856	14.93	14.86
11	2.92- 3.42	0.527	0.467	0.444	0.455	1.024	1.024	4.53×10^{-1}	4.09×10^{-1}
12	2.58- 2.92	0.490	0.392	0.406	0.416	6.65	4.96	9.35×10^{-3}	6.16×10^{-3}
13	2.09- 2.58	0.548	0.671	0.405	0.470	0.294	0.208	4.55	5.75

*Inferred from neighboring bands.

TABLE VIII

Parameters for the Broadband Opacity of N_2

	Wavelength interval (μ)	r″*	r′	r	c″	c′	c	W_c''	W_c'	W_c
1	50-100	0.999	0.993	0.997	0.402	0.422	0.420	1.295	1.266	1.268
2	29.41-50	0.998	0.933	0.974	0.174	0.272	0.260	1.972	1.628	1.612
3	17.39-29.41	0.956	0.680	0.741	1.39×10^{-2}	9.43×10^{-2}	7.15×10^{-2}	7.603	4.252	4.550
9	3.88- 4.82	0.967	0.707	0.712	2.47×10^{-2}	1.49×10^{-1}	1.46×10^{-2}	1.682	2.910	2.929

*r = s

TABLE IX

Effective Emitting Temperatures in Various Wavelength Regions

Wavelength region (μ)	Effective temperature (°K)	
	0.1% CO_2	10% CO_2
50-100	217.8	217.8
29.41-50	221.7	221.7
17.39-29.41	230.9	230.9
12.90-17.39	215.6	210.0
8.89-12.90	234.8	232.0
7.55- 8.89	234.7	234.7
5.63- 7.55	229.8	229.5
4.82- 5.63	233.0	227.8
3.88- 4.82	228.8	215.5
3.42- 3.88	234.8	233.3
2.92- 3.42	234.2	234.1
2.58- 2.92	224.2	216.4
2.09- 2.58	234.7	234.4

TABLE X

Values of Y for Various Opacity Sources*

Atmospheric level	Wavelength interval (μ)	$Y(H_2O)$	$Y(CO_2)$	$Y(N_2)$
Near cloud bottom	50-100	6.24×10^{1}		2.55×10^{-1}
Near surface		4.91×10^{5}		1.32×10^{3}
Near cloud bottom	29-50	6.54×10^{0}		3.94×10^{-2}
Near surface		4.49×10^{4}		1.78×10^{2}
Near cloud bottom	17-29	1.11×10^{-1}		1.44×10^{-3}
Near surface		9.40×10^{1}		3.76×10^{0}
Near cloud bottom	3.9-4.8	6.05×10^{-3}	3.33×10^{2}	6.25×10^{-2}
Near surface		4.23×10^{-2}	3.45×10^{3}	7.38×10^{-1}

*Cloud-bottom temperature is 240° K, cloud-top pressure 1 atm, CO_2, H_2O, and N_2 mixing ratios are 0.52, 1.7×10^{-4}, and 0.48, respectively.

TABLE XI

Summary of Model Calculations

$\tilde{P}$	T	a_{CO_2}	a_{H_2O}	a_{N_2}	P_s	M	R
0.494	240_1	> 1					
0.585	240_1	0.956	2.84×10^{-4}	0.0435	250	147	0.0260
0.790	240_1	0.747	2.13×10^{-4}	0.253	248	94.9	0.0298
1.00	240_1	0.524	1.71×10^{-4}	0.476	212	39.0	0.0428
2.05	240_1	0.153	8.53×10^{-5}	0.847	211	7.37	0.122
4.16	240_1	0.0295	4.26×10^{-5}	0.970	341	4.83	0.276
7.76	240_1	0.00477	2.27×10^{-5}	0.995	672	9.51	0.293
10.31	240_1	0.00135	1.71×10^{-5}	0.999	948	16.0	0.252
24.7	240_1	1.69×10^{-6}	6.82×10^{-6}	~1.00	2950	129	0.107
29.2	240_1	< 0					
0.266	260_1	> 1					
0.354	260_1	0.966	2.27×10^{-3}	0.0317	138	53.3	0.205
0.453	260_1	0.772	1.82×10^{-3}	0.227	127	31.7	0.241
0.612	260_1	0.501	1.40×10^{-3}	0.498	107	12.3	0.378
0.826	260_1	0.258	1.07×10^{-3}	0.741	95.4	4.69	0.773
0.982	260_1	0.173	9.09×10^{-4}	0.826	98.1	3.48	1.12
4.99	260_1	1.46×10^{-4}	1.82×10^{-4}	~1.00	403	8.42	2.83
7.43	260_1	< 0					
0.193	270_1	> 1					
0.214	270_1	0.951	7.60×10^{-3}	0.0416	77.8	23.4	0.705
0.265	270_1	0.775	6.34×10^{-3}	0.219	71.6	15.0	0.836
0.319	270_1	0.601	5.43×10^{-3}	0.394	63.6	8.84	1.09
0.378	270_1	0.431	4.75×10^{-3}	0.564	56.0	5.06	1.62
0.166	270_0	> 1					
0.187	270_0	0.904	7.22×10^{-3}	0.0888	76.5	21.0	0.731
0.212	270_0	0.814	6.58×10^{-3}	0.179	73.1	16.7	0.798
0.265	270_0	0.636	5.60×10^{-3}	0.358	65.1	9.86	1.03
0.321	270_0	0.463	4.87×10^{-3}	0.532	57.4	5.64	1.49
0.151	275_1	> 1					
0.172	275_1	0.894	1.32×10^{-2}	0.0929	55.2	14.7	1.36
0.226	275_1	0.650	1.06×10^{-2}	0.340	47.8	7.76	1.87
0.284	275_1	0.411	8.80×10^{-3}	0.580	40.0	3.87	3.24

TABLE XI

Summary of Model Calculations (Cont.)

$\tilde{P}$	T	a_{CO_2}	a_{H_2O}	a_{N_2}	P_s	M	R
0.102	275_0	> 1					
0.122	275_0	0.897	1.32×10^{-2}	0.0899	55.3	14.7	1.36
0.147	275_0	0.767	1.17×10^{-2}	0.221	51.4	10.6	1.57
0.173	275_0	0.644	1.05×10^{-2}	0.345	47.6	7.65	1.89
0.229	275_0	0.399	8.73×10^{-3}	0.592	39.6	3.74	3.36
0.113	280_1	> 1					
0.148	280_1	0.793	0.0207	0.186	38.9	9.09	2.63
0.181	280_1	0.593	0.0176	0.389	34.4	5.57	3.63
0.351	280_1	0.0973	0.0100	0.893	29.4	1.89	24.0
0.508	280_1	0.0288	0.00702	0.964	38.2	2.20	46.6
1.022	280_1	0.00162	0.00351	0.995	74.7	4.20	51.6
2.028	280_1	< 0					
0.0610	280_0	> 1					
0.0689	280_0	0.936	0.0238	0.0401	41.6	12.5	2.27
0.0781	280_0	0.867	0.0221	0.1106	40.4	10.8	2.42
0.184	280_0	0.270	0.0133	0.717	28.3	2.48	9.12
0.345	280_0	0.0545	0.00839	0.937	33.1	1.99	34.8
0.501	280_0	0.0245	0.00614	0.969	43.5	2.50	44.9
1.023	280_0	0.00124	0.00325	0.996	80.9	4.57	48.6
2.04	280_0	< 0					
0.0521	300_1	> 1					
0.0617	300_1	0.856	0.139	0.00496	12.7	5.01	16.1
0.0720	300_1	0.772	0.122	0.107	13.6	5.05	16.8
0.0860	300_1	0.541	0.108	0.351	11.4	3.09	27.0
0.0999	300_1	0.365	0.0975	0.538	10.2	2.18	45.0
0.217	300_1	0.0572	0.0488	0.894	15.5	2.47	203.0
0.330	300_1	0.0102	0.0325	0.957	22.1	3.35	367.0
0.443	300_1	< 0					

TABLE XI

Summary of Model Calculations (Cont.)

$\tilde{P}$	T	a_{CO_2}	a_{H_2O}	a_{N_2}	P_s	M	R
0.001	300_0	> 1					
0.00266	300_0	0.831	0.133	0.0353	13.1	5.09	16.2
0.00401	300_0	0.765	0.121	0.114	13.7	5.03	16.9
0.00558	300_0	0.589	0.112	0.299	11.7	3.36	24.3
0.00717	300_0	0.493	0.1051	0.402	11.12	2.82	30.4
0.0335	300_0	0.0858	0.0652	0.849	11.7	1.89	188
0.0898	300_0	0.0210	0.0423	0.937	17.1	2.60	356
0.188	300_0	0.00259	0.0282	0.969	25.4	3.82	418
0.29	300_0	< 0					
0.0375	320_1	> 1					
0.0483	320_1	0.533	0.384	0.0833	4.25	1.47	110
0.0743	320_1	0.159	0.288	0.553	4.76	1.37	499
0.0977	320_1	0.0407	0.230	0.729	6.06	1.77	1.64×10^3
0.1559	320_1	< 0					
2×10^{-5}	320_0	> 1					
1.28×10^{-4}	320_0	0.364	0.323	0.312	4.88	1.63	170
3.45×10^{-4}	320_0	0.111	0.257	0.632	5.49	1.63	682
9.70×10^{-4}	320_0	0.0249	0.210	0.766	6.87	2.08	2.08×10^3
2.21×10^{-3}	320_0	0.00496	0.179	0.816	8.68	2.83	3.26×10^3
4.5×10^{-3}	320_0	< 0					
0.0247	340_1		> 1				
0.0666	340_1	0.0237	0.636	0.341	3.27	1.42	1.69×10^4
0.0940	340_1	< 0					
7×10^{-6}	340_0		> 1				
2.80×10^{-5}	340_0	0.00263	0.599	0.398	3.76	1.78	4.50×10^3
1×10^{-4}	340_0	< 0					
8×10^{-2}	360_1		> 1				
1×10^{-1}	360_1	< 0					
7×10^{-6}	360_0		> 1				
2×10^{-5}	360_0	< 0					

TABLE XII

Model Parameters Implied by Observational Constraints

Constraints	a_{H_2O}	T(°K)	P_s †(atm)	M†	R	a_{N_2}
$a_{CO_2} \geq 0.75$; $150 \leq \tilde{P} \leq 300$ mb; wet*	3.1×10^{-3} - 1.1×10^{-2}	263-275	50-122	10-42	0.27-1.7	2.2×10^{-2} - 0.25
$a_{CO_2} \geq 0.75$; $150 \leq \tilde{P} \leq 300$ mb; dry*	3.5×10^{-3} - 2.2×10^{-2}	263-281	37-115	8-40	0.29-3.1	1.7×10^{-2} - 0.25
$a_{CO_2} = 0.97$; $\tilde{P} = 230$ mb; wet*	4.9×10^{-3}	268	100	31	0.41	2.5×10^{-2}

*Refers to type of adiabatic lapse rate within the clouds.

†A surface temperature of 700° K was used.